

Copyright Warning & Restrictions

The copyright law of the United States (Title 17, United States Code) governs the making of photocopies or other reproductions of copyrighted material.

Under certain conditions specified in the law, libraries and archives are authorized to furnish a photocopy or other reproduction. One of these specified conditions is that the photocopy or reproduction is not to be “used for any purpose other than private study, scholarship, or research.” If a user makes a request for, or later uses, a photocopy or reproduction for purposes in excess of “fair use” that user may be liable for copyright infringement,

This institution reserves the right to refuse to accept a copying order if, in its judgment, fulfillment of the order would involve violation of copyright law.

Please Note: The author retains the copyright while the New Jersey Institute of Technology reserves the right to distribute this thesis or dissertation

Printing note: If you do not wish to print this page, then select “Pages from: first page # to: last page #” on the print dialog screen

The Van Houten library has removed some of the personal information and all signatures from the approval page and biographical sketches of theses and dissertations in order to protect the identity of NJIT graduates and faculty.

ABSTRACT

EXPERIMENTALLY LINKING HEAD KINEMATICS TO BRAIN DEFORMATION

by
Imouline Algharbi

Traumatic brain injury (TBI) research is used to study the effects of brain injuries and the rehabilitations for them. TBI contributes to major cause of disability and deaths quantifying up to 30% of all the head injuries. To mimic real world impact to understand the mechanism of injury head-surrogate models are used. This thesis describes a method to record head kinematics from acceleration and angular rate sensors of head-brain surrogate model for blast and blunt injury. This methodology is validated through experimental testing. To get a better insight of the head kinematics experienced by a real skull a drop tower is used to delivered controlled impacts to the head model. The loading conditions include velocities at 1.3, and 1.5 m/s, impact locations at the crown and the forehead of the skull and with the brain composition being a 20% ballistics gelatin. The output head kinematics were then combined with brain deformation data and linked to head injury criteria. The strain, accelerometer and angular rate measurements were done using NI cDAQ-9188 Data Acquisition System combined with LabVIEW. Then, the data was analyzed in MATLAB.

**EXPERIMENTALLY LINKING HEAD KINEMATICS TO BRAIN
DEFORMATION**

**by
Imouline Algharbi**

**A Thesis
Submitted to the Faculty of
New Jersey Institute of Technology
in Partial Fulfillment of the Requirements for the Degree of
Master of Science in Biomedical Engineering**

Department of Biomedical Engineering

August 2019

APPROVAL PAGE

**EXPERIMENTALLY LINKING HEAD KINEMATICS TO BRAIN
DEFORMATION**

Imouline Algharbi

Dr. Bryan J. Pfister, Thesis Advisor Date
Professor and Chair of Department of Biomedical Engineering, NJIT

Dr. Namas Chandra, Committee Member Date
Distinguished Professor of Biomedical Engineering, NJIT

Dr. Saikat Pal, Committee Member Date
Associate Professor of Biomedical Engineering, NJIT

BIOGRAPHICAL SKETCH

Author: Imouline Algharbi

Degree: Master of Science

Date: August 2019

Undergraduate and Graduate Education:

- Master of Science in Biomedical Engineering,
New Jersey Institute of Technology, Newark, NJ, USA 2019
- Bachelor of Science in Biomedical Engineering,
New Jersey Institute of Technology, Newark, NJ, USA 2017
- Associate of Science in Computer Science,
Bergen Community College, Paramus, NJ, USA 2015

Major: Biomedical Engineering

This thesis is dedicated to my family and friends. Their support and influence is why I made it this far.

ACKNOWLEDGMENT

I would like to thank my thesis advisor, Dr. Bryan Pfister, for inviting me to work with him. Dr. Pfister's constant support and expert suggestions. I will always appreciate the opportunity that I had to participate and learn from CIBM3 because of him. I would like to extend my thanks to Dr. Namas Chandra and Dr. Saikat Pal to be part of the committee members. I would also like to thank Abdus Ali, Prasad Vijay Bhatambarekar and Jose Rodrigues for helping me with my research and gathering data. Finally, I would like to acknowledge my parents, family and friends for supporting me throughout my academic career.

TABLE OF CONTENTS

Chapter	Page
1 INTRODUCTION.....	1
1.1 Introduction of Traumatic Brain Injury.....	1
1.2 Mechanics of Brain Injury.....	2
1.3 Injury Criteria and Thresholds	2
1.4 Research Aims.....	4
2 METHODOLOGY.....	5
2.1 Skull Modeling	5
2.2 Simulated Brain.....	6
2.3 Acceleration of a Rigid Body.....	10
2.4 Strain Gage.....	12
2.5 Accelerometer.....	14
2.6 Angular Rate Sensor.....	17
2.7 Data Acquisition System.....	20
2.8 LabView Programming.....	21
2.8.1 LabVIEW Program Structure.....	22
2.9 MATLAB Programming.....	22
2.10 Drop Tower.....	23
2.11 High Speed Video Recording.....	24
2.12 Brain Deformation Analysis.....	25

TABLE OF CONTENTS
(Continued)

Chapter	Page
2.13 Wiring Diagram.....	26
3 RESULTS AND DISUCSSION.....	29
3.1 Accelerometer Validation Experiment.....	30
3.2 Accelerometer Comparison.....	32
3.3 Accelerometer Results.....	36
3.4 Angular Rate Sensor Results.....	44
3.5 Strain Gage Results.....	50
3.6 HIC.....	56
4 CONCLUSION AND FUTURE WORK.....	59
APPENDIX A STRAIN GAGE VALIDATION EXPERIMENT.....	62
APPENDIX B MATLAB SCRIPT 1.....	64
APPENDIX C LABVIEW PROGRAM.....	73
APPENDIX D MATLAB SCRIPT 2.....	77
REFERENCES	81

LIST OF TABLES

Table	Page
2.1 Summary of Experimental Parameters	24
3.1 Validation Experiments Results.....	31
3.2 Comparison Experiment Results.....	35
3.3 X-axis Acceleration Results at Different Impact Speed.....	37
3.4 Y-axis Acceleration Results at Different Impact Speed.....	39
3.5 Z-axis Acceleration Results at Different Impact Speed.....	41
3.6 X-axis Angular Velocity Results at Different Impact Speed.....	45
3.7 Y-axis Angular Velocity Results at Different Impact Speed.....	47
3.8 Z-axis Angular Velocity Results at Different Impact Speed.....	49
3.9 Skull Front Results at Different Impact Speed.....	53
3.10 Skull Rear Results at Different Impact Speed.....	53
3.11 Skull Crown Results at Different Impact Speed.....	53
3.12 HIC Results Skull Rear Results at Different Impact Speed.....	58

LIST OF FIGURES

Figure	Page
2.1 Production of ballistic gelatin brains.....	6
2.2 Blunt Impact Experimental Setup (front view).	8
2.3 Blunt Impact Experimental Setup (side view).....	9
2.4 Sensor Mounting Scheme	12
2.5 Three wire circuit strain gages.	13
2.6 ADXL377 Functional Block Diagram.	16
2.7 Endevco 7264C Functional Block Diagram.....	17
2.8 DTS ARS PRO-18k Angular Rate Sensor.	18
2.9 Skull 3D model with sensors mounted in the y and z axes	19
2.10 Skull 3D model with sensors mounted in the x axis.	20
2.11 Motion tracked deformation grid.....	26
2.12 Wiring diagram of the three different type of sensors.	27
2.13 Image of the drop tower with the sensors mounted and wired properly	28
3.1 Accelerometer Validation Experiment in the Z-axis.....	30
3.2 Accelerometer Validation Experiment in the Y-axis.....	30
3.3 Graph of acceleration (m/s ²) vs. time (sec) shows a comparison between ADXL377 and Endevco accelerometer in the x-axis during 1.5m/s impact speed.	32
3.4 Graph of acceleration (m/s ²) vs. time (sec) shows a comparison between ADXL377 and Endevco accelerometer in the y-axis during 1.5m/s impact speed.	33

3.5	Graph of acceleration (m/s ²) vs. time (sec) shows a comparison between ADXL377 and Endevco accelerometer in the z-axis during 1.5m/s impact speed.	34
3.6	Graph of acceleration (m/s ²) vs. time (sec) shows acceleration in the x-axis during 1.5m/s impact.	36
3.7	Graph of acceleration (m/s ²) vs. time (sec) shows acceleration in the x-axis during 1.3 m/s impact.	36
3.8	Graph of acceleration (m/s ²) vs. time (sec) shows acceleration in the y-axis during 1.5m/s impact.	38
3.9	Graph of acceleration (m/s ²) vs. time (sec) shows acceleration in the y-axis during 1.3m/s impact.	38
3.10	Graph of acceleration (m/s ²) vs. time (sec) shows acceleration in the Z-axis during 1.5m/s impact.	40
3.11	Graph of acceleration (m/s ²) vs. time (sec) shows acceleration in the Z-axis during 1.3m/s impact.....	40
3.12	Graph of acceleration (m/s ²) vs. time (sec) shows a comparison between all the axis during 1.5m/s impact speed.	42
3.13	Graph of acceleration (m/s ²) vs. time (sec) shows a comparison between all the axis during 1.3m/s impact speed.	42
3.14	Graph of angular velocity (degree/sec) vs. time (sec) shows angular velocity in the X-axis during 1.5m/s impact.	44
3.15	Graph of angular velocity (degree/sec) vs. time (sec) shows angular velocity in the X-axis during 1.3m/s impact.	44
3.16	Graph of angular velocity (degree/sec) vs. time (sec) shows angular velocity in the Y-axis during 1.5m/s impact.	46
3.17	Graph of angular velocity (degree/sec) vs. time (sec) shows angular velocity in the Y-axis during 1.3m/s impact.	46
3.18	Graph of angular velocity (degree/sec) vs. time (sec) shows angular velocity in the Z-axis during 1.5m/s impact.....	48
3.19	Graph of angular velocity (degree/sec) vs. time (sec) shows angular velocity in the Z-axis during 1.3m/s impact.	48

3.20	Graph of strain vs. time (sec) shows strain in the front of the skull during 1.5m/s impact.....	50
3.21	Graph of strain vs. time (sec) shows strain in the front of the skull during 1.3m/s impact.	50
3.22	Graph of strain vs. time (sec) shows strain in the rear of the skull during 1.5m/s impact.....	51
3.23	Graph of strain vs. time (sec) shows strain in the rear of the skull during 1.3m/s impact.....	51
3.24	Graph of strain vs. time (sec) shows strain in the crown of the skull during 1.5m/s impact.....	52
3.25	Graph of strain vs. time (sec) shows strain in the crown of the skull during 1.3m/s impact.....	52
3.26	Graph of strain vs. time (sec) shows a strain comparison between the front, crown and rear areas of the skull during 1.5m/s impact.....	54
3.27	Graph of strain vs. time (sec) shows a strain comparison between the front, crown and rear areas of the skull during 1.3m/s impact.	54
3.28	Heat maps generated from MATLAB script.....	55

CHAPTER 1

INTRODUCTION

1.1 Introduction to Traumatic Brain Injury

Traumatic brain injury (TBI) refers to brain abnormality caused by force applied to the head. TBI is one of the most common injuries in the United States. Studies have shown that more than 5 million people are affected with TBI [1]. Traumatic brain injury has been identified as a major health concern by the U.S. Center for Disease Control and Prevention and 75% of reported incidents are categorized as concussion or mild [2]. There are two types of TBI closed and open. Closed TBI refers to an injury without any physical damage to the skull, while an open TBI refers to skull breaking and damage to the brain. Traumatic Brain Injury is a serious health issue that is definitely worth understanding in order to prevent it and treat patients [5].

Traumatic Brain Injury research is used to study the effects of brain injuries and the rehabilitations for them. There are many ways to study TBI. Some devices induce a non-penetrating traumatic brain injury or blunt injury, and some induce a penetrating injury on animals. Most devices give the user independent control over injury parameters such as velocity, distance, depth and dwell time across wide range of velocity contributes to reliability and accuracy of brain injury as a model of TBI [3].

1.2 Mechanics of Brain Injury

Depending on the mechanism and forces involved in a brain injury, structural changes due to the injury may be microscopic. The brain is the primary concern in a head injury, whether it is affected through direct or indirect injury mechanisms. There are layers of bone and tissue surrounding the brain, that act to prevent and minimize brain injury. If the layers are severely damaged, they cause rather than prevent brain injury.

Injuries are classified as open and closed injuries. Open injury involve penetration to the scalp, skull and usually meninges and underlying brain tissues. The skull fracture may be a hairline fracture, where the broken piece moves towards the brain, or a compound fracture when the skull breaks into several pieces and cuts into the scalp. Closed injury occurs when the head is struck or shaken violently, causing rapid brain acceleration and deceleration. “Acceleration or deceleration can injure tissue at the point of impact, at its opposite pole, or diffusely; the frontal and temporal lobes are particularly vulnerable to this type of injury. Axons, blood vessels, or both can be sheared and torn, resulting in diffuse axonal injury. Disrupted blood vessels leak, causing contusions, intracerebral or subarachnoid hemorrhage, and epidural or subdural hematomas” [4].

The mechanical behavior and clinical outcomes differ depending on the injury mode. Understanding the effects of each injury mode is outside the scope of this work, but the focus will be on blunt injuries or closed injury. When the skull experiences an impact by blunt object, it tends to move faster than the viscoelastic brain which is still stationary at the time of impact producing compressive wave at the site of impact before propagating to the brain [6].

1.3 Injury Criteria and Thresholds

In an attempt to better understand how hard an impact must be to cause severe head injury, injury criteria have been developed to analyze the head kinematics. To obtain collision data, tests are performed in circumstances similar to the environment that is being investigated. Various injury criteria exist for assessing different types of injuries. These criteria contain structural imaging, loss of consciousness, post-traumatic amnesia, Glasgow Coma Scale (GCS), and Abbreviated Injury Scale score (AIS). Head Injury Criteria ((HIC) is used by the National Highway Traffic Safety Administration (NHTSA) in rating vehicle safety [5]. HIC is defined as

$$HIC = \left\{ \left[\frac{1}{t_2 - t_1} \int_{t_1}^{t_2} a(t) dt \right]^{2.5} (t_2 - t_1) \right\}_{max} \quad (1.1)$$

Where $a(t)$ is the resultant linear acceleration, and t_1 , and t_2 are the start and end times for the duration where the highest HIC values are generated. The duration is usually 15ms or 36ms. The HIC has been used in many applications to prevent severe head injuries. Rapid acceleration of the head can be caused by a range of activities. For example, it may contain vehicle accidents, falls from playground, heavy tackles or encounters in contact sport. In situations where there is a high possibility that the head will be dramatically decelerated, design measures need to be taken to ensure that damage to the brain is minimized. To properly account for safety in design it is desirable to be able to analyze the potential lethality of the situation which has caused the collision. This is achieved by using test apparatus with appropriate measuring equipment, performing tests to get suitable collision data and analyzing the impact

data. To develop and update the values, experiments have been performed on animals, finite element model and head surrogate models [7].

1.4 Research Aim

The purpose of this study is to evaluate an instrumented model as a research device for measuring in-vivo head impact kinematics at the center of gravity of the skull. To evaluate kinematics accuracy, laboratory impact testing was performed on a surrogate model and the motion was recorded via a high-speed recording camera for determining how closely instrumented the device data matched data from the high-speed camera. The model includes six degree of freedom kinematics measurements. Three degrees of freedom are linear accelerations and the other three are angular velocities. Skull deformation was measured using strain gauges.

CHAPTER 2

METHODOLOGY

2.1 Skull Modeling

In previous studies, a PVC skull was used from Anatomy Warehouse to simulate the human skull. The interest now is more focused on understanding the deformation that occurs at different sections of the head along with the head kinematics. The process required to get PVC skull working required a lot of mechanical effort and precision such as portion of the skulls had to be excised. One of the disadvantages using this skull was that it had tiny holes that are required to fix to ensure the simulated brain does not leak through it. Additionally, the skull lacked a mounting base, therefore ½ inch polycarbonate plate was made like metal plate and appropriate holes were to be drilled.

To overcome the inefficient process, a CAD model (half skull) was designed and developed using PTC Creo Parametric software. The CAD model was then 3D printed and soaked in a 2% Sodium Hydroxide and water solution to degrade the support material that the printer leaves. The skull was soaked overnight with the solution and then the skull was treated with de-ionized water to neutralize the chemical reaction. For this study, a previous worked on model was used as printing a new model is unnecessary. However, the model was modified for the purpose of this study. Skull's center of gravity (CG) was calculated through PTC Creo Parametric software and the three axes (x, y and z) were projected orthogonally to CG. In the YZ plane two marks were added in y and z axes at the surface of the skull to track the motion of a rigid body acceleration.

2.2 Simulated Brain

The brain was mimicked using 20% ballistic gelatin melted and poured into the skull cavity. The gel is manufactured by Clear Ballistics. The gel is melted and then poured into the skull as per the manufacture instructions. The gel is melted between 121°C (250°F) to 132°C (270°F) and settled down for 12 hours. Due to the skull not having a definite shape entity, a base was made to pour the gel in a levelled manner. The hot gel led to bubbles formation at the surface. To get rid of the bubbles a vacuum chamber was used. It took about 10 seconds to pull vacuum through the chamber and 90 seconds for the bubbles pop out, and then the vacuum was released to allow air back into the chamber. All remaining bubbles were removed manually.

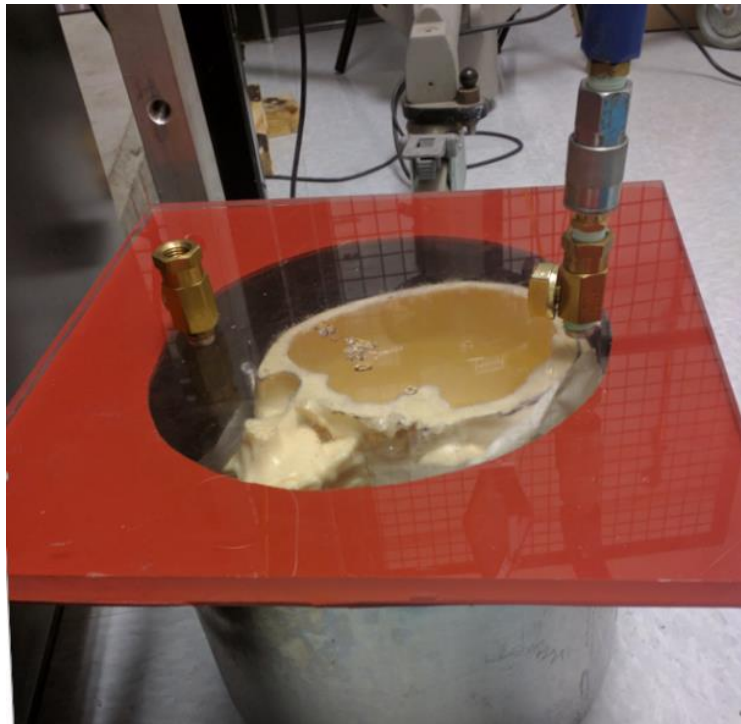


Figure 2.1 Production of ballistic gelatin brains.

Note: Head model is placed inside a metal pot, with a polycarbonate sheet with a silicone ring (red) to seal the edges. The protrusion on the right side of the surface connects a tube to a vacuum to remove air from the container, pulling out bubbles.

A 3D printed grid was used to create a marker array on the surface on the brain surrogate. The grid was prepared by Abdus Ali. The reason behind the grid of markers is to be able to track the motion of the markers by a high-speed camera to capture the deformation of the gel/brain surrogate. The grid separated the centers of each marker by 0.375mm, with the grid laying on the gel, a black acrylic spray paint was used to form black markers on the gel surface. The painted gel was allowed to dry for at least 4 hours before the final layer of gel can be poured. For the purpose of this experiment, two marks were added near each of the accelerometer that are mounted on the surface of the skull to track the motion at the site of the accelerometers using the high-speed camera.

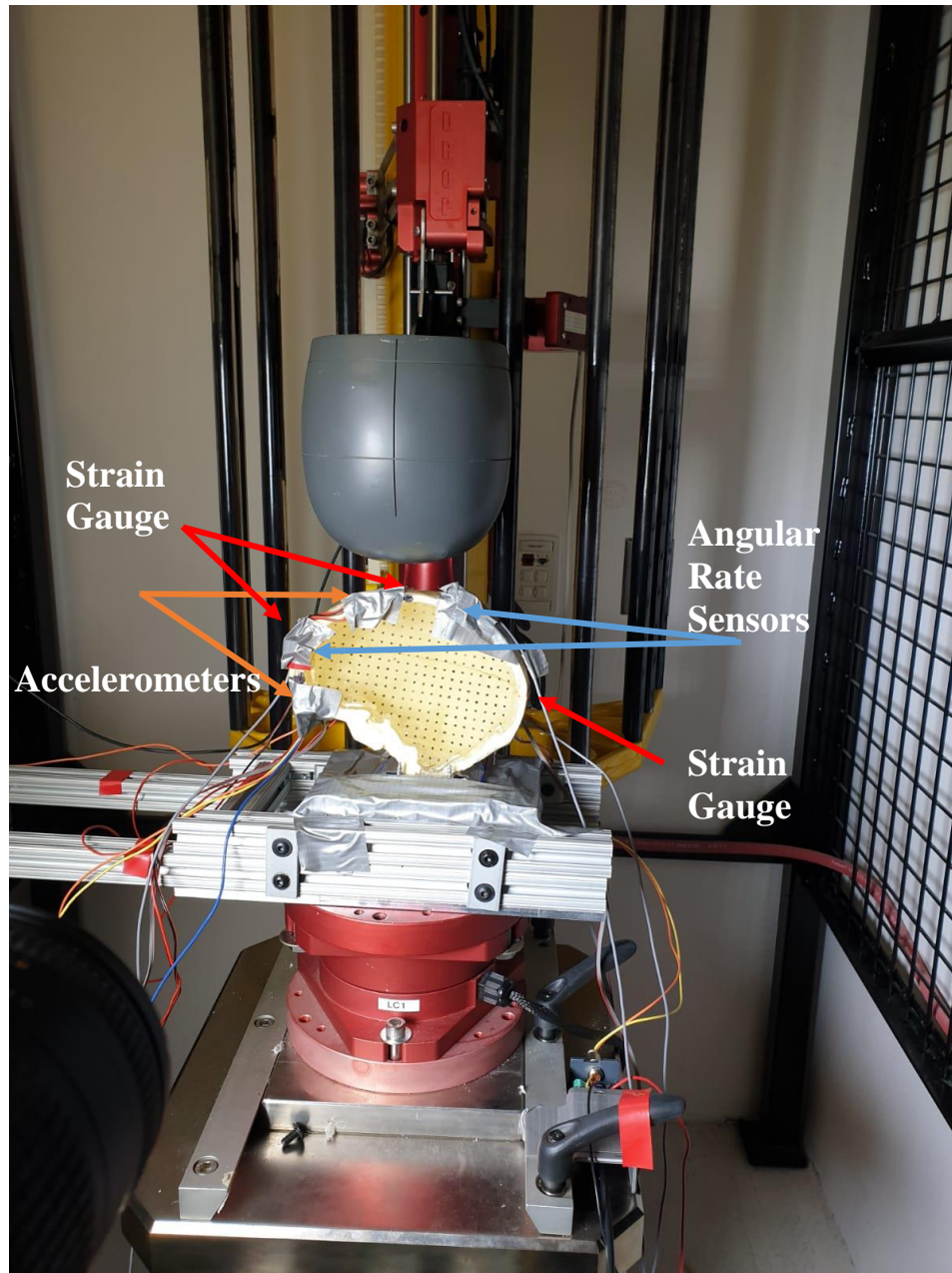


Figure 2.2 Blunt Impact Experimental Setup (front view).

The head model is sitting on such that the linear impactor (grey) will contact the skull at the crown. The orange arrows in the figure are pointing out to the accelerometers, the blue arrows are point out to the angular rate sensors and the red arrows are pointing out to the strain gauges

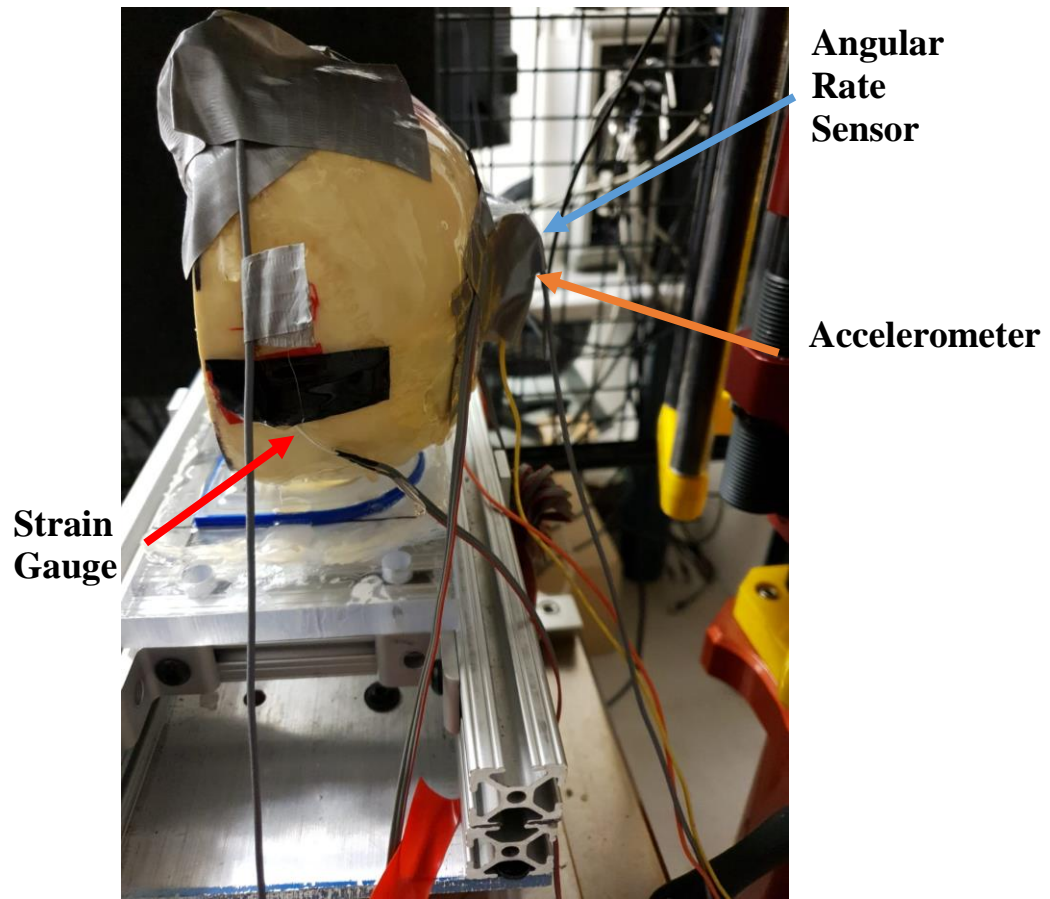


Figure 2.3 Blunt Impact Experimental Setup (side view).

The orange arrows in the figure are pointing out to the accelerometers, the blue is pointing out to the angular rate sensor.

2.3 Acceleration of a Rigid Body

In biomechanical research with cadavers and anthropomorphic test dummies, head acceleration must be measured to determine brain injury risk during motor vehicle safety tests. Rigid body acceleration at the center of the head determines the Head Injury Criteria (HIC) value. Angular head motion is also used as an injury criterion. This has promoted efforts to measure the six degree of freedom acceleration of a rigid body.

It was proved that if the linear acceleration of a point on a rigid body is desired, then it is possible by mounting three orthogonal linear accelerometers near the point. However, if the point is internal, then the sensors cannot be mounted nearby. The acceleration of such an inaccessible point can still be determined by measuring the acceleration of a second point on the rigid body as a reference point at any convenient location, along with the angular velocity and angular acceleration of the rigid body. In this study the inaccessible point is the center of gravity of the skull and the reference point was the center of gravity projected to the surface of the skull. The center of gravity of the model was calculated in PTC Creo Parametric Software. In an equation form the acceleration of the reference point is expressed as

$$\vec{A}_p = \vec{A}_0 + \vec{\omega} \times (\vec{\omega} \times \vec{r}_p) + \dot{\vec{\omega}} \times \vec{r}_p \quad (2.1)$$

where: \vec{A}_p – acceleration of the reference point, P, on the rigid body with respect to the inertial frame; \vec{A}_0 – acceleration of the origin, 0, of the body-fixed reference frame with respect to the inertial frame; $\vec{\omega}$ – angular velocity of the rigid body frame;

$\vec{\dot{w}}$ – angular acceleration of the rigid body frame; \vec{r}_p – position of point, P, with respect to the origin, 0, of the body-fixed frame [10].

The sensors that are needed to measure the acceleration of an inaccessible point (point 0 in fig 2.1) within the rigid body become evident when Eq. (1) is separated into x, y, and z components:

$$\vec{A}_{0x} = \vec{A}_{px} + r_x(w_y^2 + w_z^2) - r_y(w_y w_x - \dot{w}_z) - r_z(w_z w_x - \dot{w}_y) \quad (2.2)$$

$$\vec{A}_{0y} = \vec{A}_{py} + r_y(w_x^2 + w_z^2) - r_x(w_y w_x + \dot{w}_z) - r_z(w_z w_y - \dot{w}_x) \quad (2.3)$$

$$\vec{A}_{0z} = \vec{A}_{pz} + r_z(w_x^2 + w_y^2) - r_x(w_y w_z - \dot{w}_y) - r_y(w_z w_y + \dot{w}_x) \quad (2.4)$$

A method was developed by (Martin,Crandall) to measure the acceleration of the inaccessible point within the rigid body using three accelerometers and three angular rate sensors. Under this scheme, the centripetal acceleration and the linear acceleration along the coordinate axes at the peripheral points (points 1, 2, and 3 in Fig. 2.4) are the only measurements needed to determine the linear acceleration of the inaccessible point (point 0 in Fig. 2.4). Thus, only six sensors are required: three accelerometers (the boldfaced vectors in Fig. 2.4) and the three sensors within the ARS cube. As such, Equations (2)– (4) are reduced so that acceleration at the inaccessible point may be found from Equations (5)– (7) [8].

$$A_{0x} = A_{1x} + r_x(w_y^2 + w_z^2) \quad (2.5)$$

$$A_{0Y} = A_{2Y} + r_Y(w_X^2 + w_Z^2) \quad (2.6)$$

$$A_{0Z} = A_{3Z} + r_Z(w_X^2 + w_Y^2) \quad (2.7)$$

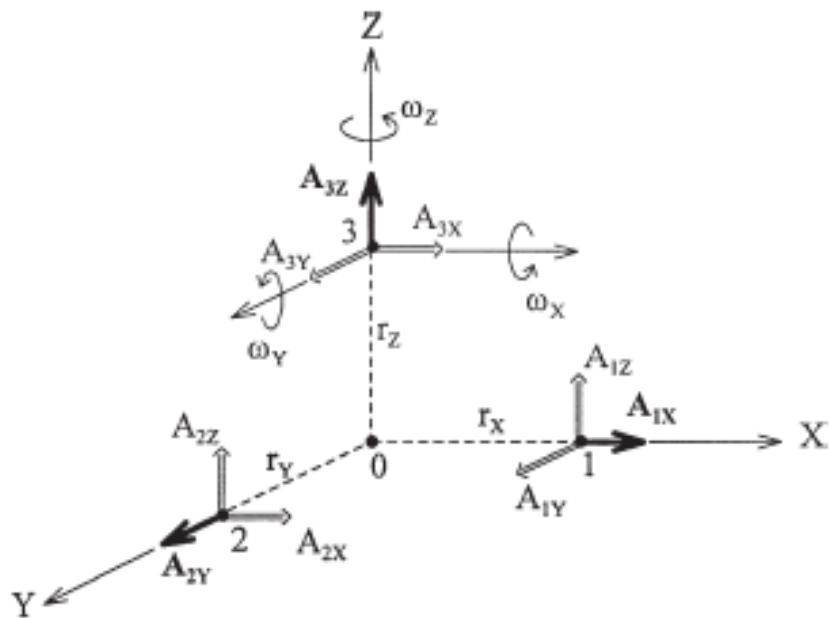


Figure 2.4 Sensor Mounting Scheme.

Source: Martin, P. et al (1998) Measuring the acceleration of a rigid body 1-15

2.4 Strain Gauge

When a fine wire is strained within its elastic limit, the wire's resistance changes because of changes in the diameter, length and resistivity. The resulting strain gauges may be used to measure extremely small displacements on the order of nanometers. The strain gauge is a metallic foil which works on the principle of resistance change which is measured using a Wheatstone bridge and is related to strain by the quantity known as Gauge Factor. Gauge Factor (G) is the measure of sensitivity, or output,

produced by a resistance strain gauge. Gauge factor is determined through calibration of the specific gauge type and is the ratio between $\Delta R/R_0$ and $\Delta L/L$ (strain), where R_0 is the initial unstrained resistance of the gauge. The four sets of strain-sensitive wires are connected to form a Wheatstone bridge (figure 2.2). In this study, strain gauges of 350Ω (ohms) resistance 3-wire were used, Omega KFH-6-350-C1-11L3M3R. The 350Ω strain gauge provide better heat dissipation, decrease the lead wire effects and improve signal to noise ratio [OMEGA].

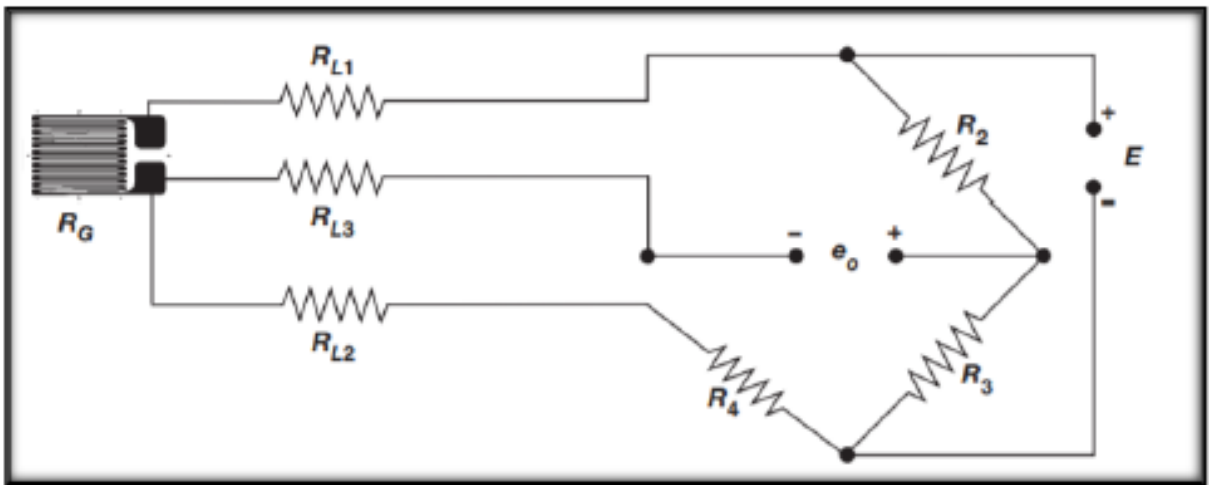


Figure 2.5 Three Wire Circuit Strain Gauge.

Source: www.micro-measurements.com, Vishay Precision Instruments, revised July 14, 2015, Document number 11092.

The strain gauges have to be mounted on the surface in a specific way. The gauges are glued to the surface of the model. Prior to gluing, the surface has to be cleaned thoroughly with alcohol and acetone to get rid of any debris on the placement location. The upper side of the gauge has a marking which helps in alignment. Based on the principle of the gauges, if the area of foils narrows, then the resistance increases which represent tension experienced by the gauge, while if the area

expands, then the resistance decreases due to compression experienced by the gauge.

To validate the strain gauge measurements, an initial experiment on cantilever beam was conducted by Prasad Bhatambarekar, a former lab colleague (Experiment details are in Appendix A) [10].

2.5 Accelerometer

An Accelerometer is an apparatus, either mechanical or electrochemical for measuring acceleration or deceleration, which is the rate of increase or decrease in the velocity of a moving object. An accelerometer is a device that measures the vibration, or acceleration of motion of a structure. The force caused by vibration or a change in motion (acceleration) causes the mass to "squeeze" the piezoelectric material which produces an electrical charge that is proportional to the force exerted upon it. Since the charge is proportional to the force, and the mass is a constant, then the charge is also proportional to the acceleration. Accelerometers measure in meters per second squared (m/s^2) or in G-forces (g). A single G-force for us here on planet Earth is equivalent to $9.8 m/s^2$, but this does vary slightly with elevation. The type of sensors used to measure acceleration, shock or tilt include piezo film, electromechanical servo, piezoelectric, bulk micro-machined piezo-resistive, capacitive and surface micro-machined capacitive. Each sensor has distinct characteristic in output signal, development cost, and type of operating environment in which its best functions [11].

Accelerometers can measure acceleration on one, two, or three axes. 3-axis units are becoming more common as the cost of development for them decreases. Generally, accelerometers contain capacitive plates internally. Some of these are fixed,

while others are attached to minuscule springs that move internally as acceleration forces act upon the sensor. As these plates move in relation to each other, the capacitance between them changes. From these changes in capacitance, the acceleration can be determined. Other accelerometers can be centered around piezoelectric materials. These tiny crystal structures output electrical charge when placed under mechanical stress (e.g. acceleration) [11].

For this study, two accelerometers were compared ADXL377 and Endevco 7264C. ADXL377 is a small, thin, low power, complete 3-axis accelerometer (ADXL377) with signal conditioned analog voltage outputs that has a full-scale range of $\pm 200g$ with no signal saturation. This measurement range, combined with an analog output that continuously captures impact data, make the ADXL377 an ideal sensor for contact sports where the detection of concussive forces can reveal indicators of TBI, with a bandwidth of 1600H [12].

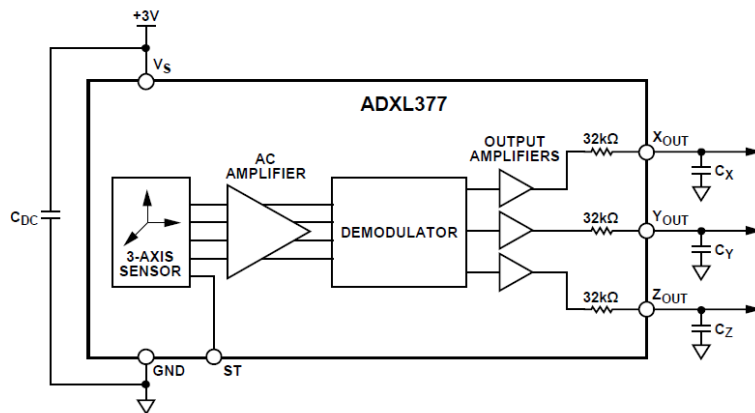


Figure 2.6 ADXL377 Functional Block Diagram.

Source: www.analog.com

Endevco 7264C is piezoresistive accelerometer. The Endevco is a very low mass accelerometer. This accelerometer is designed for crash testing, rough road testing. It has a full-scale range of $\pm 2000g$ with a maximum frequency of 4000Hz [13]. However, the price of the Endevco sensor is 23 times the price of ADXL377. To compare the results of each accelerometer an experiment was carried out with 1.5m/s impact speed. The Endevco accelerometers were placed near the ADXL377. Raw accelerometer measurements were filtered using a second-order Butterworth low-pass filter with a cutoff frequency of 200Hz. The reason behind choosing 200Hz as a cutoff frequency is because a Fast Fourier Transformer (FFT) was computed in MATLAB on the raw data.

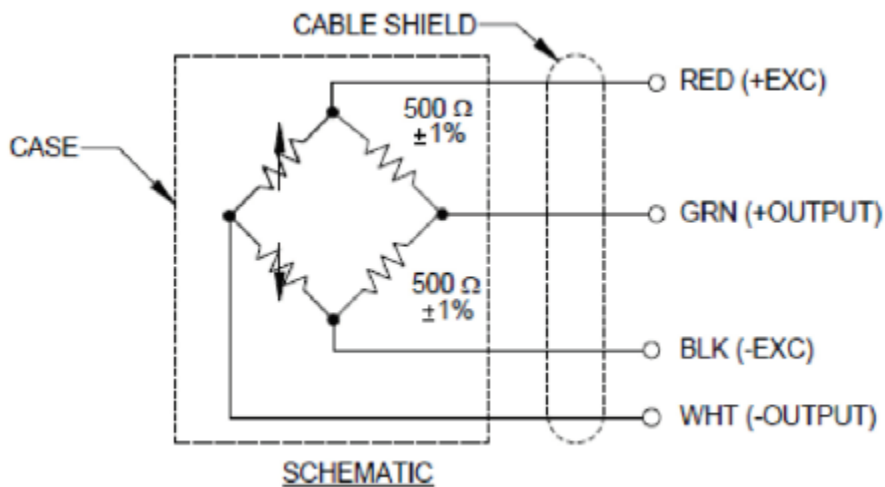


Figure 2.7 Endevco 7264C Functional Block Diagram.

Source: <https://buy.endevco.com/7264c-accelerometer.html>

To validate the accelerometer measurement, an initial experiment on the skull model was carried out. Two accelerometers were mounted on the skull on two axes (YZ plane). Two dots were placed on the skull near accelerometers using a black marker. The motion of the accelerometers was captured in LabVIEW as voltage vs. time data in excel spreadsheets. The spreadsheets were then loaded into MATLAB.

The MATLAB script (Appendix B) filtered raw accelerometers using a notch filter at 60Hz and using a second-order Butterworth low-pass filter with a cutoff frequency of 200 Hz. Then, the linear acceleration was converted to m/s^2 . The linear velocities were obtained by integrating the linear acceleration using cumulative trapezoidal numerical integration method using MATLAB. The motion of the selected dots was captured using ProAnalyst's 2D tracking feature. For each video, brightness and contrast were adjusted to help the motion tracking algorithm's accuracy. All resulting motion-tracked data was inspected visually to correct for tracking errors the software may have made.

The 2D tracked marker data was exported from ProAnalyst as dot numbers and its respective location based on coordinate system over time in excel spreadsheets. The spreadsheets were loaded into MATLAB. The MATLAB script (Appendix C) differentiated the markers displacement measurements to velocity (m/s) and then accelerations (m/s^2). The acceleration graphs of the accelerometer measurements were compared to the marker's acceleration graph.

2.6 Angular Rate Sensor

Angular rate sensors, while not an entirely new technology, have become more reliable and 'ultra-small and low mass' [14] where they can be easily placed in objects of interest with limited space. For this paper will use angular rate sensors (DTS ARS PRO-18k), measuring angular velocity. DTS ARS PRO angular rate sensors are ultra-small, low mass single axis rate sensors that has a full-scale range of $\pm 18000 \text{ deg/sec}$ ($\pm 314.2 \text{ rad/sec}$) and is shock rated to 10,000g with a bandwidth of 2000Hz.

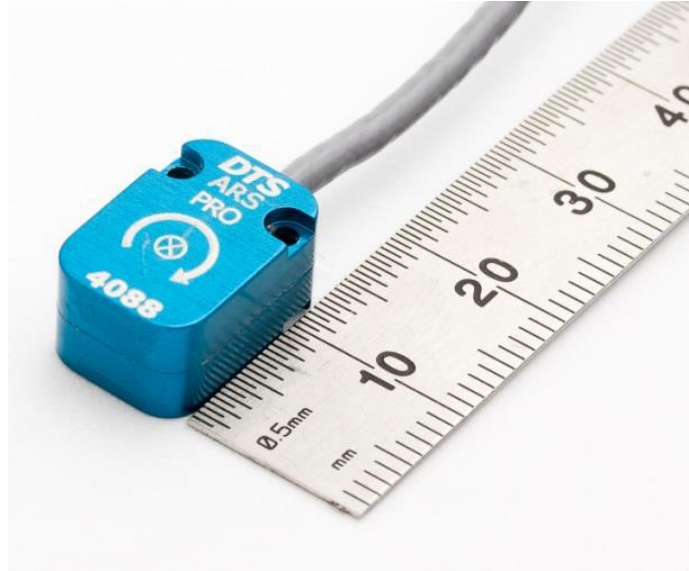


Figure 2.8 DTS ARS PRO-18k Angular Rate Sensor.
Source: www.dtsweb.com/angular-rate-ars-pro-hg/

Figures 2.9 and 2.10 illustrate how the accelerometers were placed on the skull model. As discussed earlier the center of gravity was calculated using PTC Creo. The center of gravity was projected to the surface of the skull and the axes were projected to the surface of the skull where the sensors are mounted. The orange dot is the center of gravity while the green lines are the three orthogonal axes projected from the center of gravity. To secure the sensor on the skull, a piece of duct tape was placed on top of the sensors.

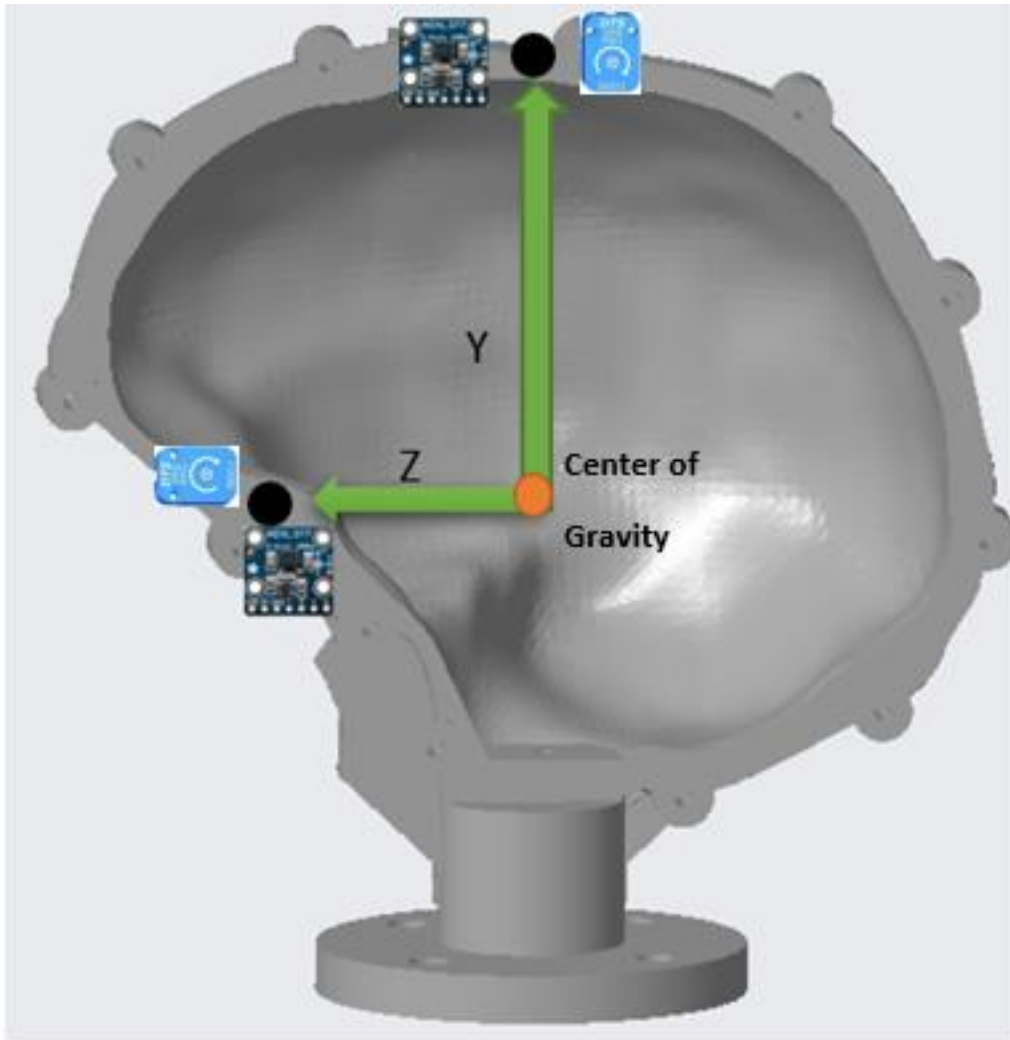


Figure 2.9 Skull 3D model with sensors mounted in the y and z axes.

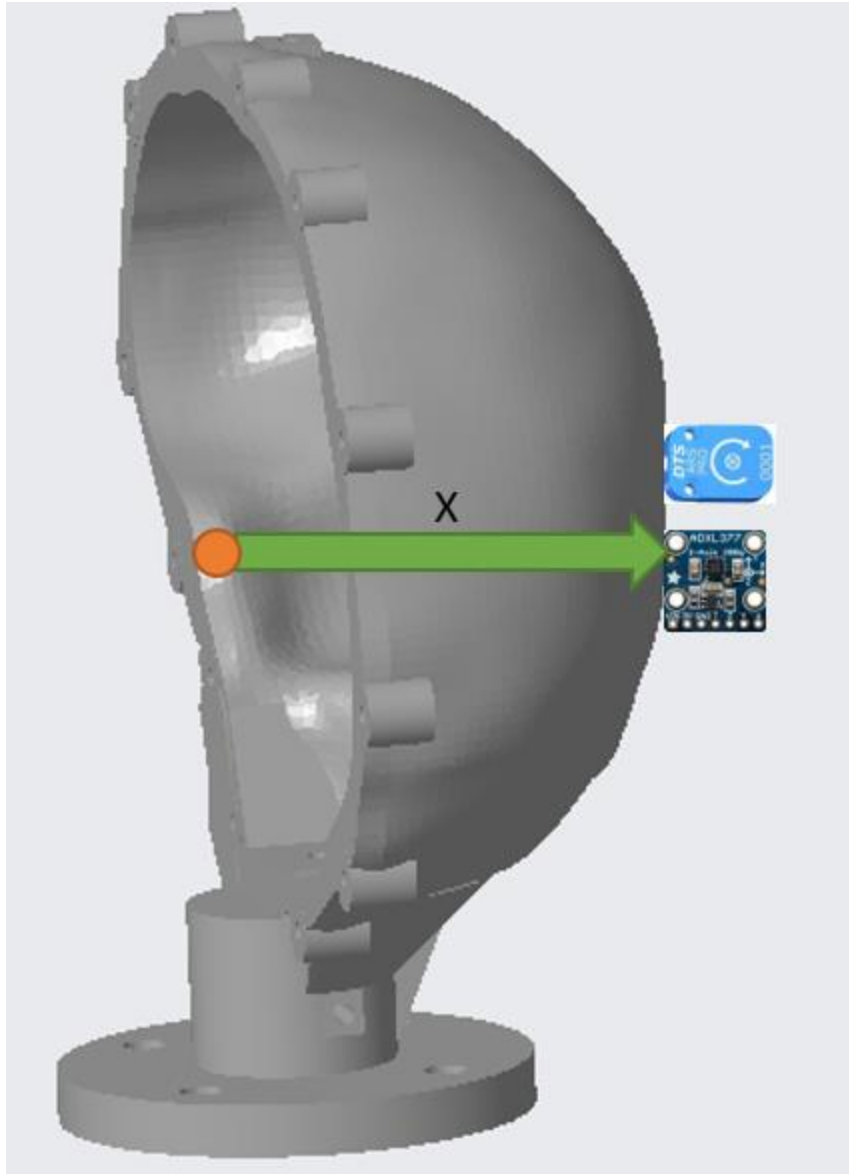


Figure 2.10 Skull 3D model with sensors mounted in the x axis.

2.7 Data Acquisition System

The data recording and analysis was carried out using National Instrument's Compact Data Acquisition Chassis (NI cDAQ-9188) along with NI-9188, and NI-9218, a module that is designed for multipurpose measurement. It offers built-in support for accelerometer, powered sensor, full-bridge, and voltage measurements as well as quarter bridge, half bridge, 60V and current measurement using measurement specific adapters.

Each channel is individually selectable, which allows performing multiple measurement at once. The NI-9218 is a 51.2 kS/s/ch, 2-Channel C Series Universal Analog Input Module.

A LabVIEW code was developed to record the accelerometers and angular rate sensor data. The sensors were configured as voltage measurements to allow multiple channels of different sensors in one code.

2.8 LabVIEW Programming

LabVIEW stands for **L**aboratory **V**irtual **I**nstrument **E**ngineering **W**orkbench is a graphical programming environment you can use to develop sophisticated measurement, test, and control systems. LabVIEW is an open environment which is designed to interface with any kind of hardware measurement. LabVIEW was developed by National Instruments (NI), which so far has been successfully used for data acquisition and control. LabVIEW unlike other software which are based on text coding, uses graphical form of coding to develop a data flow diagram. A data flow diagram which makes it highly interactive and easy at use. LabVIEW can also be referred to as Application Specific Development Environment. Its high level rapid development environment for measurement and automation application makes it the most popular software in data acquisition.

The components of LabVIEW are based on Virtual Instrumentation commonly referred to as "VI". The concept of "Virtual Instrumentation" is the keystone of the LabVIEW environment. A virtual instrument consists of an industry-standard computer equipped with powerful application software written in LabVIEW, cost-effective hardware such as plug-in modules.

LabVIEW provides two working environments, one for the graphical user interface which is called the front panel. The front panel contains the controls, indicators such as buttons, sliders, dials, tables, graphs etc. The other environment is the block diagram. Every front panel object has a terminal in the block diagram and the programmer wires the terminal to functions that are illustrated as icons to determine the flow of data throughout the program which can function as hardware buttons to perform desired actions. Therefore, it eliminates the code syntax as other software which make LabVIEW increase the productivity and decrease the required time to develop the application [17].

2.8.1 LabVIEW Program Structure

As discussed before, data flow determines the sequence of execution in LabVIEW. In this program all the events in the program are handled by an event structure. The event structure is a structure resembling a case structure that has a case associated with each event. By using a while loop the event structure waits for an event to occur, executes code to respond to the event, and reiterates to wait for the next event. Every action of the software suit such as performing data acquisition. Snippets of the program is in appendix B.

2.9 MATLAB Programming

MATLAB stands for **Matrix Laboratory**. MATLAB is a multi-numerical computing environment and proprietary programming language developed by MathWorks. MATLAB allow the user for matrix manipulation, plotting function, and data implantation. MATLAB supports developing application with graphical user interface

(GUI) features. Two MATLAB scripts were designed for the purpose of this study. First script is designed to filter accelerometer raw data that was captured via LabVIEW, then convert the filtered raw data from voltage (V) to acceleration (m/s^2), then integrate the acceleration to velocity (m/s). Lastly the first script plot acceleration and velocity vs. time. The second script was designed to plot the displacement data of the dots motion that was captured via ProAnalyst, then the data is differentiated to velocity (m/s), and then the velocity is differentiated to acceleration(m/s^2).

2.10 Drop Tower

To replicate real-world blunt impact, a free fall guided, uniaxial impact monorail was used (1000_00_MIMA). This machine is developed by Cadex Inc. Testing Equipment, Canada. The drop tower consists of a projectile impactor which weighs around 10 pounds- close to the human skull, the impactor is pneumatically actuated. To measure the drop height an electronic encoder is used. To determine the velocity of an impact, a time gate (infrared beam based) sensor is used. It also consists of an accelerometer the measure the impact acceleration using Newton's second law, additionally calculating the Head Injury Criterion [8]. The base consists of load cells which determine the force experienced by the model. The drop tower has preset variable impact speed and relative height setting viz, 3, 5 and 7mph.

In this experiment, tests were performed at 1.3, and 1.5 m/s. The impact location is the crown while the impact speed was varied to link the relation between head kinematics by measuring the acceleration and the angular velocity and brain deformation by measuring stain on the skull model. 3 trials of each were recorded.

Table 2.1 Summary of Experimental Parameters

Location	Crown	
Velocity	1.3m/s	1.5 m/s
Drop Height	12 cm	14 cm
Number of trials	3	3
Sensors used	Accelerometers x3 angular rate sensors x3 strain gauges x2	

2.11 High Speed Video Recording

The various injury events were captured using a high-speed camera (UX100 M3 camera by Photron, USA) recording at 4000 fps. The camera was set to be facing perpendicular to the surface of the viewing window, ensuring that the viewing angle would not cause a distorted view of the motion of the markers.

To study the effects of impact accurately, the high-speed camera was used. When slowing down the footage by shooting high frame rate, it is necessary to consider the required increase in exposure. Shooting at high frame rates requires substantial lighting levels. As the number of frames per seconds doubles, the amount of light required to achieve the same exposure also doubles. A grid of led lights was used which provided sufficient lighting, to reduce the effect of glare since the gel and window are reflective surfaces, a proper angle must be set up.

2.12 Brain Deformation Analysis

To track the grid movement during and after the impact, 2D tracking of the marked dot was performed using ProAnalyst software. For each video, brightness and contrast were adjusted to help the motion tracking algorithm's accuracy. The software is based on Continuum theory which requires known reference location coordinates between two points. Each dot is being tracked individual region. Some of the dots fail to be tracked algorithmically due to the changes in the shape of the gel during the impact. The dots can be then manually tracked individually per frame by adjusting the brightness and contrast of.

The 2D tracked marker data was exported from ProAnalyst as marker numbers and its respective location in an arbitrary but consistent coordinate system over time in excel spreadsheets. These spreadsheets were then loaded into MATLAB. A custom script (Appendix D) was developed at CIBM3 was used to analyze the data.

To closely understand the effects of brain deformation regional mapping was performed. The region consisted of one square containing 4 points which sums up 220 points.

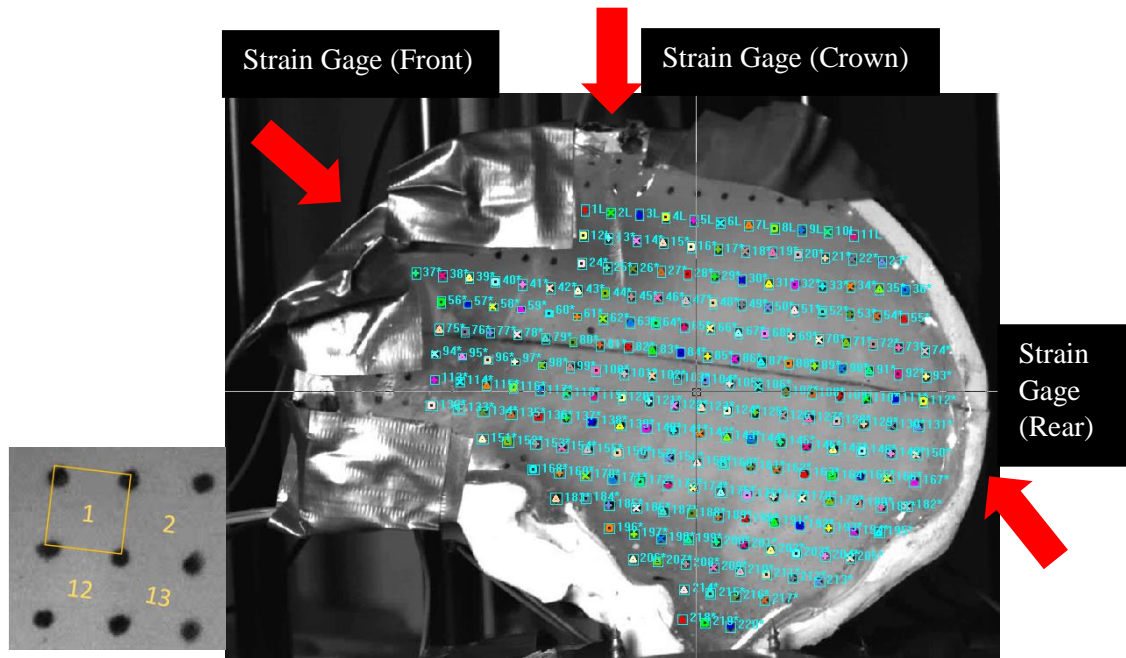


Figure 2.11 Motion tracked deformation grid.

(A) The four black dots at the corners of the yellow box indicate user-defined markers, which are motion tracked. (B) 220 points within the marked grid.

2.13 Wiring Diagram

Figure 2.12 illustrates wiring diagram of all the sensors. Accelerometers (ADXL377) are excited externally with 3VDC power supply through pin 3V and ground (GND), angular rate sensors (ARS DTS PRO-18K) are excited externally with 5VDC power supply through + Excitation and – Excitation wires, while the strain gauges are excited internally with 2.5VDC through National Instruments modules (NI 9237). Figure 2.13 shows the experimental setup with all the sensors and wiring connected.

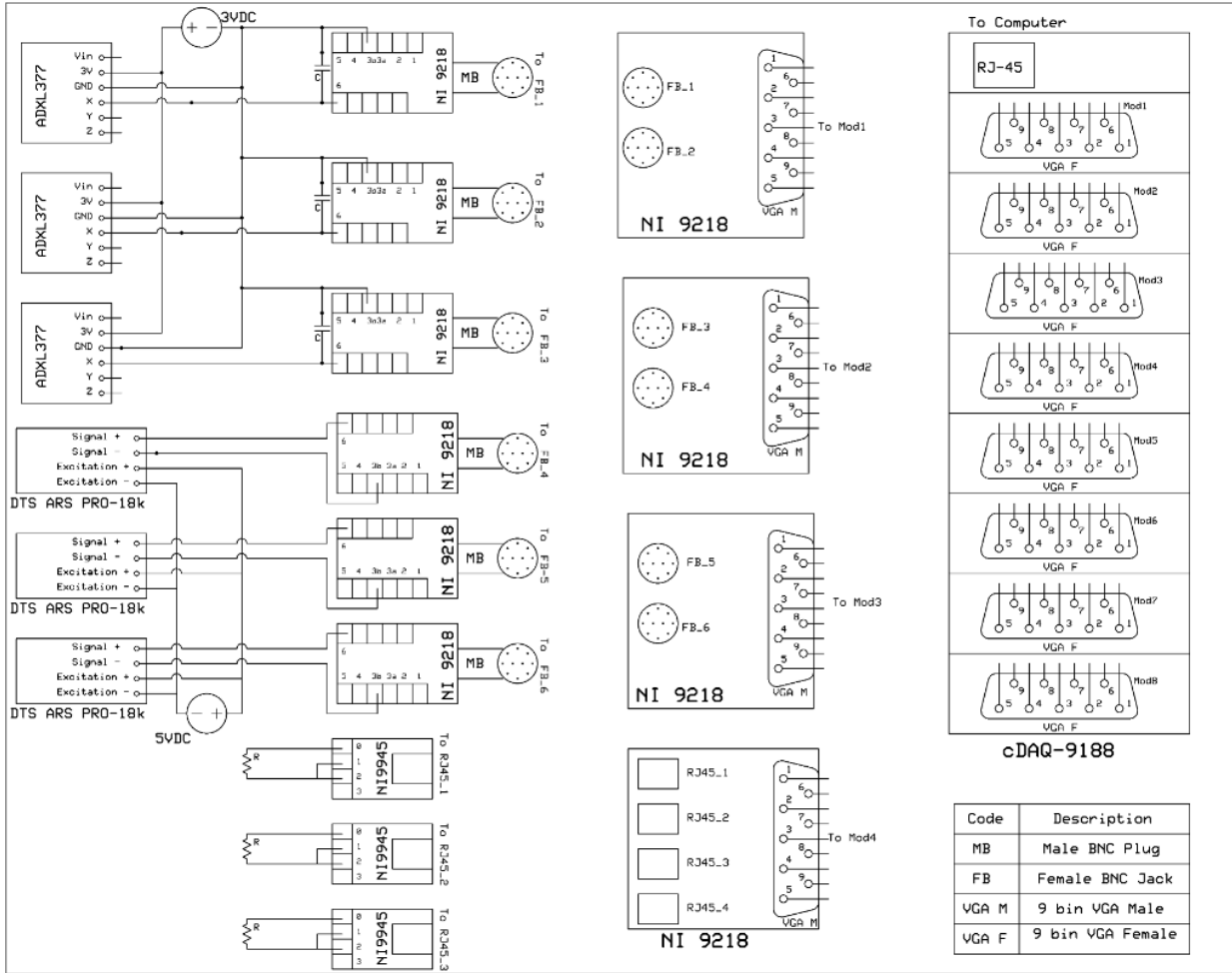


Figure 2.12 Wiring diagram of the three different type of sensors.

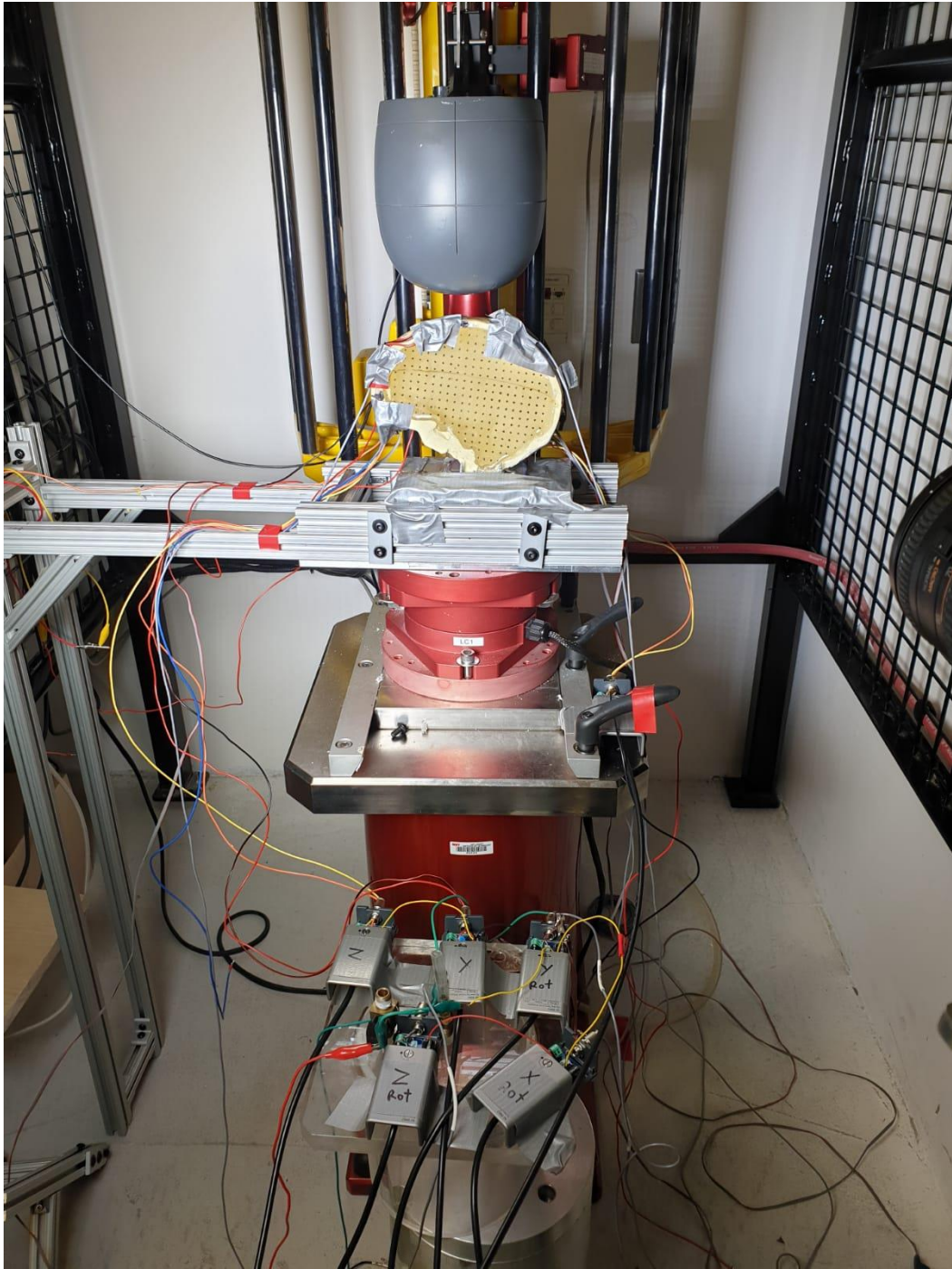


Figure 2.13 Image of the drop tower with the sensors mounted and wired properly.

CHAPTER 3

RESULTS AND DISCUSSION

To evaluate the repeatability and thereby reliability, multiple drops of 1.3 and 1.5m/s (3 of each in each impact location) were performed. The results from strain gauge, accelerometers and angular rate sensors were recorded in the form of numerical values, exported to an excel spreadsheets and analyzed in MATLAB. Strain gauges values can be theoretically obtained as a voltage measurement which will need to be converted. However, LabVIEW has a built-in function that provided strain values instead of voltage which eliminate the need for conversion. Unfortunately, this is not the case for the accelerometers and the angular rate sensors. The latest sensors have different sensitivities and different configurations which made it easier to record the data as a voltage and then convert the values to m/s^2 and degree/sec in MATALB. In other words, the data from the three different sensors were recorded using two LabVIEW codes and analyzed using two different MATALB scripts.

For clarity, the results were plotted and summarized in tables, and all readings were averaged to determine consistency. Motion tracking of marker grid helped in analyzing the spatial as well as regional deformation or strain experienced by the gel. Heat maps generated from MATLAB code helped in determining the location of concentration of each nature of strain- tensile, compressive and shear.

3.1 Accelerometer Validation experiment

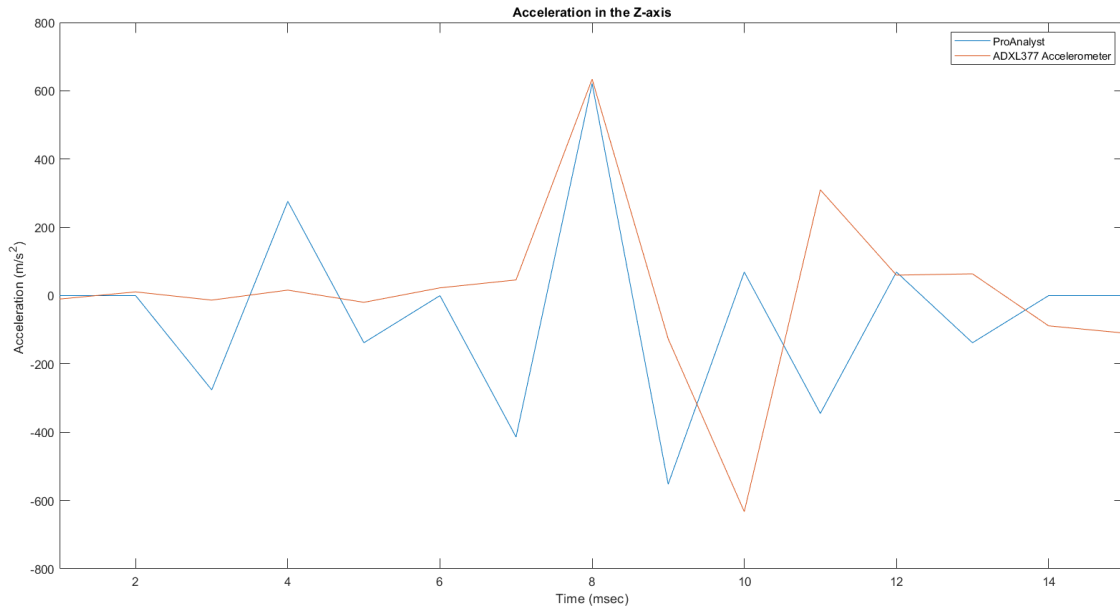


Figure 3.1 Accelerometer Validation Experiment in the Z-axis.

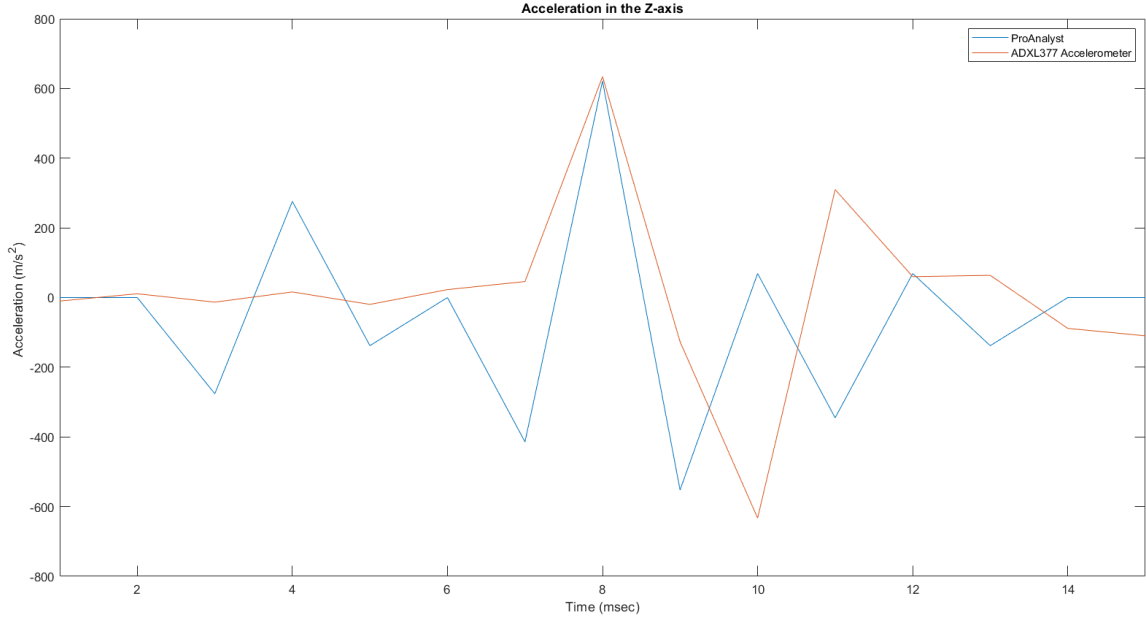


Figure 3.2 Accelerometer Validation Experiment in the Y-axis.

The validation experiment was conducted to validate the accelerometer measurement. The 2D tracked marker data was exported from ProAnalyst as displacement measurements in excel spreadsheets. The spreadsheets were loaded into MATLAB and differentiated to obtain velocity and acceleration data. The acceleration data from MATLAB were compared to accelerometer measurements after exporting LabVIEW data and filtering the raw accelerometer measurements. Figures 3.1 and 3.2 illustrate the acceleration graphs of in the z and y axes. ProAnalyst results and accelerometer results are within 2% error in the z-axis and 4.4% error in the y-axis. The percent error was calculated based on the equation 3.1. Since the percent error is below 5%, that means the percent error is acceptable and the accelerometer data are validated. Table 3.1 summarizes the results from the validation experiments. This short experiment helped in much better understanding of the accelerometer, their handling, positioning and thereby confirming the use of accelerometer code that was developed.

$$\text{Percent Error} = \left| \frac{\text{ProAnalyst Value} - \text{Experimental Value}}{\text{ProAnalyst Value}} \right| \times 100 \quad (3.1)$$

Table 3.1 Validation Experiment Results

Data		ProAnalyst	Experimental	Percent Difference
Acceleration m/s ² (g)	Z-axis	621 (63)	634 (64)	2%
	Y-axis	714 (72)	746 (76)	4%

3.2 Accelerometer Comparison

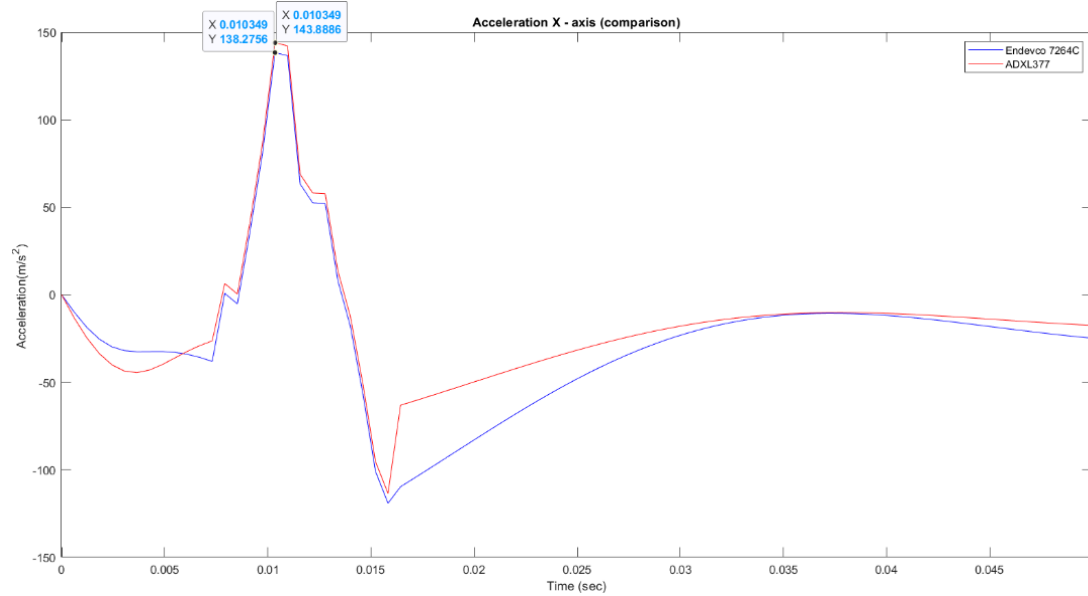


Figure 3.3 Graph of acceleration (m/s²) vs. time (sec) shows a comparison between ADXL377 and Endevo accelerometers in the x-axis during 1.5m/s impact speed.

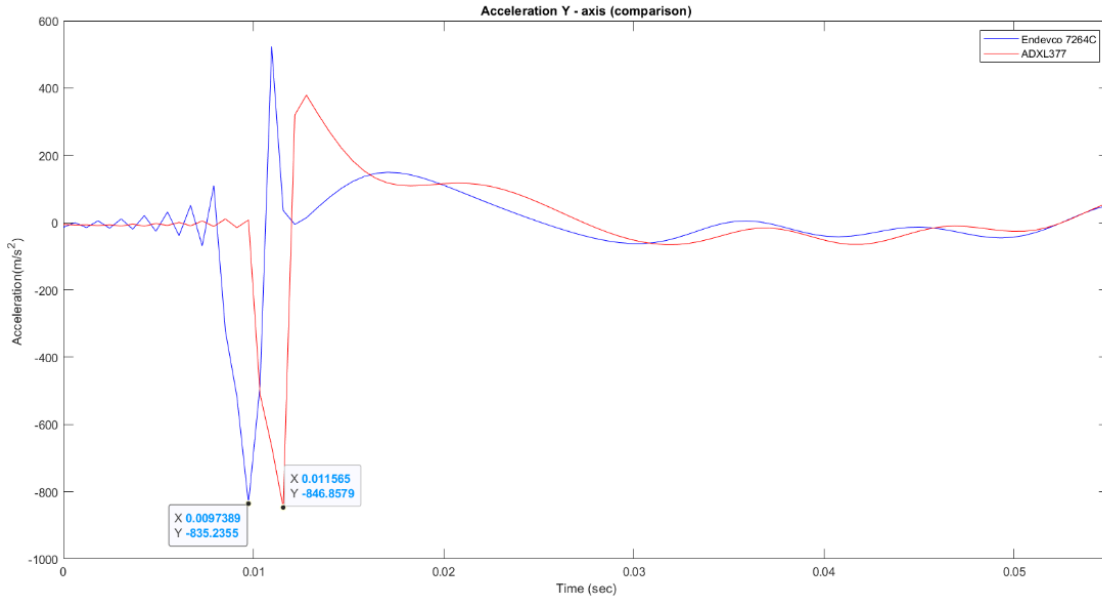


Figure 3.4 Graph of acceleration (m/s^2) vs. time (sec) shows a comparison between ADXL377 and Endevo accelerometers in the y-axis during 1.5m/s impact speed.

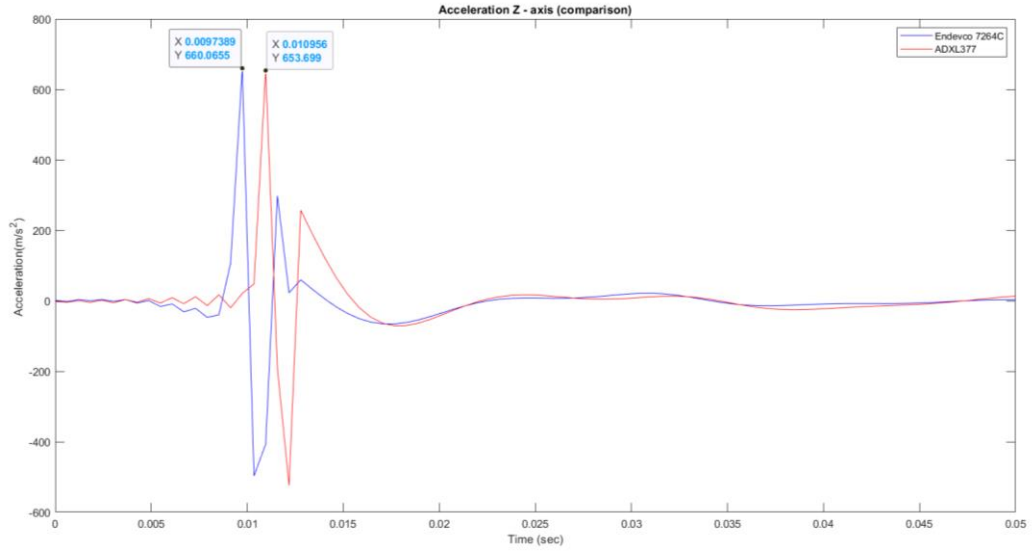


Figure 3.5 Graph of acceleration (m/s^2) vs. time (sec) shows a comparison between ADXL377 and Endevo accelerometers in the z-axis during 1.5m/s impact speed.

ADXL377 accelerometers measurements were compared to Endevco measurements in all three axes during a 1.5m/s impact speed and recoded in figures 3.3. 3.4 and 3.5. Some of the graph are plotted with a time delay on purpose to show the difference between the two different measurements from the accelerometers. Figure 3.5 shows the comparison in the z-axis with a percent difference of 3% and 1.3% difference in the y-axis, and the least percent difference in the x-axis with 1%. The percent difference was calculated based on equation (3.2). The percent difference between the two types of accelerometers is insignificant meaning that the two accelerometers can be used in such an experiment and will results in very much alike results. The take home message from this experiment is that it is not necessary to use costly sensors to get accurate results. However, precise results can still be achieved using economical sensors. Since the two accelerometers are comparable, the rest of the experiments will be conducted using ADXL377 accelerometer.

$$\text{Percent Difference} = \frac{|Value1 - Value2|}{\left[\frac{Value1 + Value2}{2}\right]} \times 100 \quad (3.2)$$

Table 3.2 Comparison Experiment Results

Data		Endevco 7246	ADXL 377	Percent Difference
Acceleration m/s ² (g)	Z-axis	138.1 (14)	146 (14.8)	3%
	Y-axis	-835 (-85)	-846 (-86.3)	1.3%
	X-axis	660 (67.3)	653 (66.6)	1%

3.3 Accelerometer Results

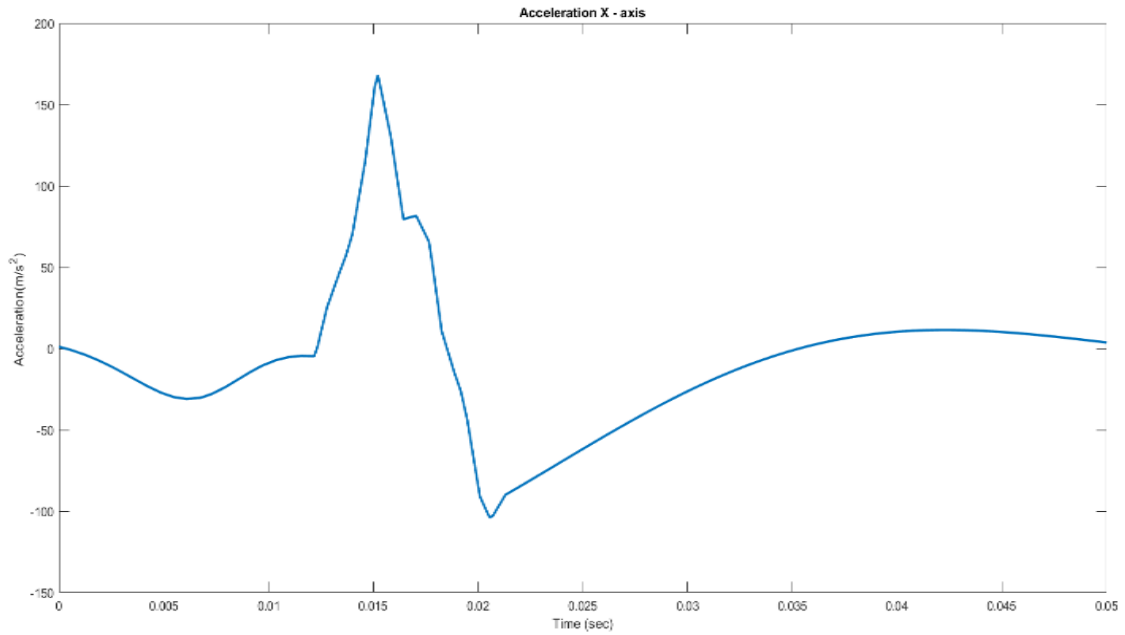


Figure 3.6 Graph of acceleration (m/s^2) vs. time (sec) shows acceleration in the x-axis during 1.3m/s impact.

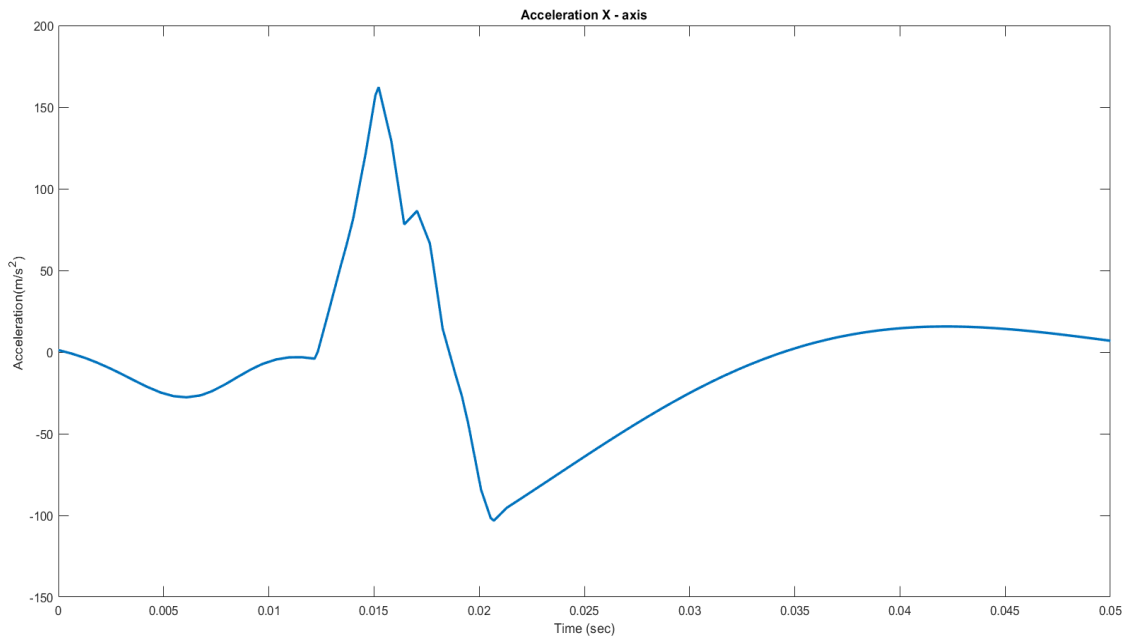


Figure 3.7 Graph of acceleration (m/s^2) vs. time (sec) shows acceleration in the x-axis during 1.5 m/s impact.

Figure 3.6 illustrates graph of acceleration vs. time recorded from impact at the crown with an impact speed of 1.3m/s in the x-axis. Accelerometer shows positive peak acceleration of 168 m/s² (17 g). In the beginning of the graph the graph shows negative acceleration to flexion in the skull, while later the graph shows positive acceleration in the x-axis followed by deceleration, and then the graph returns to zero meaning the skull is returning to original position.

Figure 3.7 illustrates graph of acceleration vs. time recorded from impact at the crown with an impact speed of 1.5m/s in the x-axis. Accelerometer shows positive peak acceleration of 162 m/s² (16.2 g). The first negative peak suggests skull flexion experienced by the skull as the skull starts to accelerate. As the skull continues to accelerate there is a significant change in slope of the graph indicated by the peak generated in the positive direction which is the maximum acceleration experienced by the skull in the x-axis followed by another change in the slope of the graph suggesting the deceleration skull while returning to its original position. Table 3.3 shows a summary of acceleration results of the three trials in the x-axis with 1.3 and 1.5m/s impact speed. The percent difference of in table 3.1 means that the acceleration in the x-axis during the two impact speeds is identical.

Table 3.3 X-axis Acceleration Results at Different Impact Speed.

Impact Speed		1.5 m/s	1.3m/s
Acceleration	Trial 1	168.1 m/s ² (17.1 g)	162.2 m/s ² (16.5 g)
	Trial 2	150 m/s ² (15.3 g)	157 m/s ² (16.0 g)
	Trial 3	149.7 m/s ² (15.3 g)	148 m/s ² (15.1 g)
Average		155.9 m/s ² (15.9 g)	155.7 m/s ² (15.9 g)
Percent Difference		0.13%	

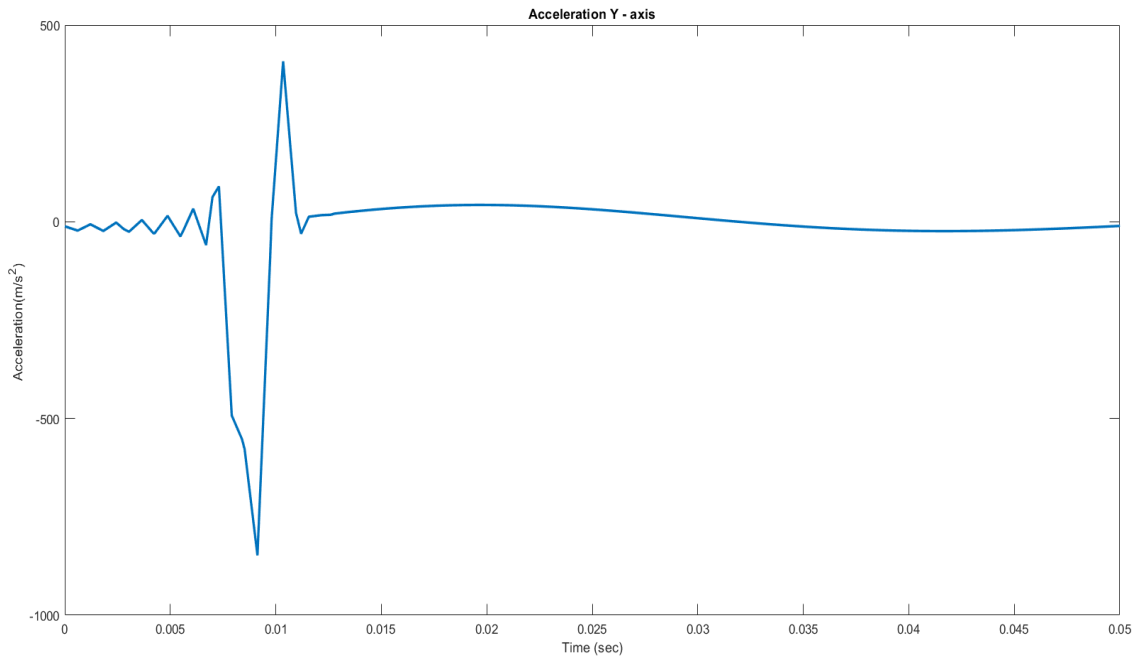


Figure 3.8 Graph of acceleration (m/s^2) vs. time (sec) shows acceleration in the y-axis during 1.3m/s impact.

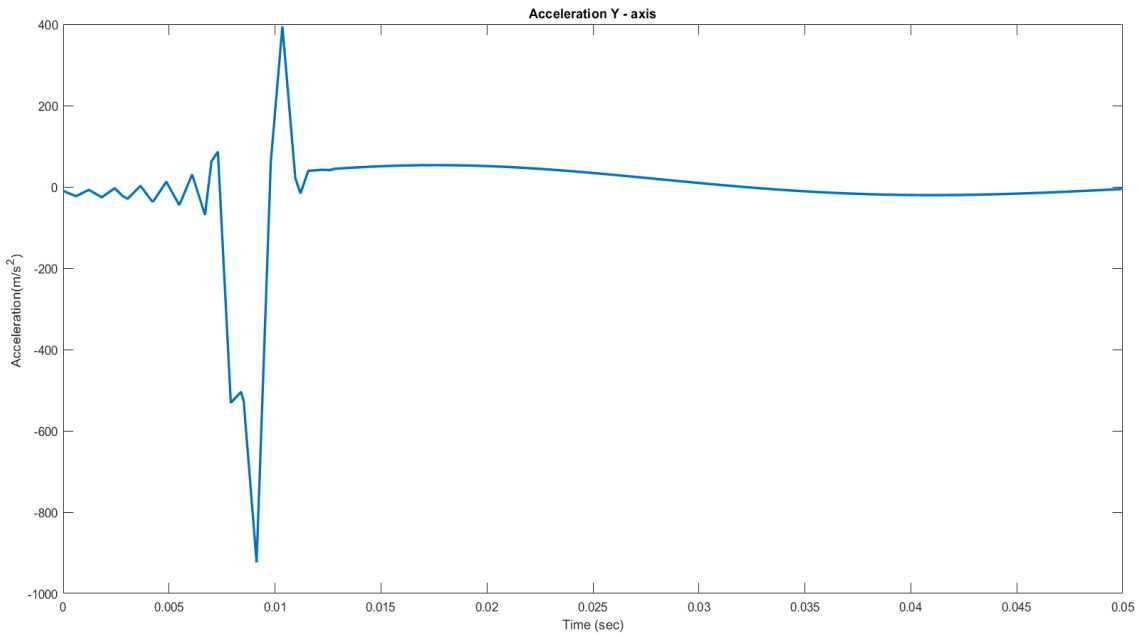


Figure 3.9 Graph of acceleration (m/s^2) vs. time (sec) shows acceleration in the y-axis during 1.5m/s impact.

Figure 3.8 illustrates graph of acceleration vs. time recorded from impact at the crown with an impact speed of 1.3m/s in the y-axis. Accelerometer shows negative peak acceleration of -847.9 m/s^2 (-86.5 g). The first few oscillations suggest vibration experienced by the accelerometer as the skull start to accelerate. As the skull continues to accelerate there is a significant change in slope of the graph indicated by the peak generated in the negative direction which suggest the maximum acceleration experienced by the skull in the negative direction.

Figure 3.9 illustrates graph of acceleration vs. time recorded from impact at the crown with an impact speed of 1.5m/s in the y-axis. Accelerometer shows a negative peak acceleration of -923.7 m/s^2 (-94.2 g). The first few oscillations suggest vibration experienced by the accelerometer as the skull start to accelerate, followed by acceleration of the skull in the negative direction and then deceleration until the skull returns to it is original position. Table 3.4 shows acceleration results of the three trials in the y-axis with 1.3 and 1.5m/s impact speeds. The percent difference suggests that the acceleration increases with the increase of the impact speed across the y-axis.

Table 3.4 Y-axis Acceleration Results at Different Impact Speed.

Impact Speed		1.5 m/s	1.3 m/s
Acceleration	Trial 1	-923.7 m/s^2 (-94.2 g)	-847.9 m/s^2 (-86.5 g)
	Trial 2	-889 m/s^2 (-90.7 g)	-728 m/s^2 (-74.2 g)
	Trial 3	-717 m/s^2 (-73.1 g)	-675 m/s^2 (-68.8 g)
Average		-843.2 m/s^2 (-86.0g)	-750.3 m/s^2 (-76.5 g)
Percent Difference		11.7%	

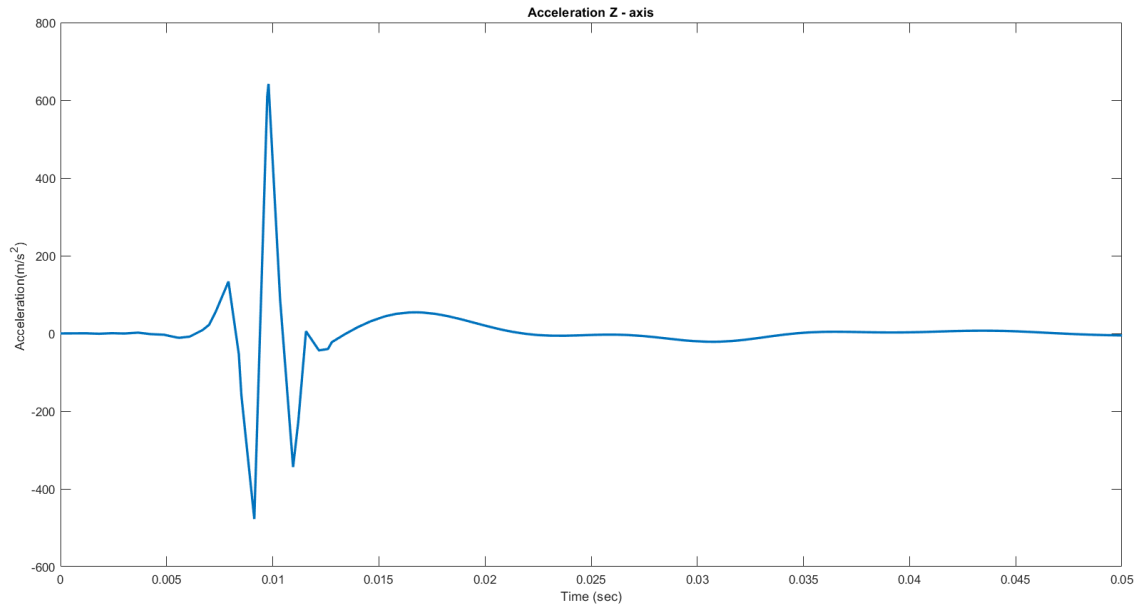


Figure 3.10 Graph of acceleration (m/s^2) vs. time (sec) shows acceleration in the Z-axis during 1.3m/s impact.

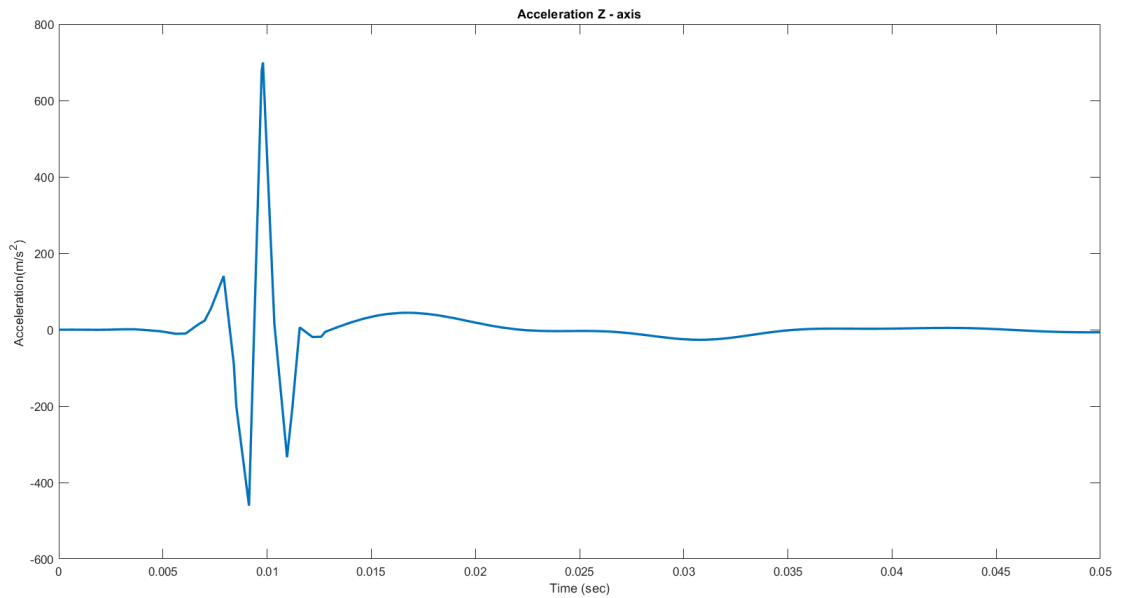


Figure 3.11 Graph of acceleration (m/s^2) vs. time (sec) shows acceleration in the Z-axis during 1.5m/s impact.

Figure 3.10 illustrates graph of acceleration vs. time recorded from impact at the crown with an impact speed of 1.3m/s in the z-axis. Accelerometer shows positive peak acceleration of 642 m/s² (65.5 g). In the beginning of the graph, the graph shows negative acceleration due to flexion in the skull, followed by a noticeable change in the slant of the graph to represent the acceleration of the skull, after that the graph starts deaccelerating while the skull is deaccelerating.

Figure 3.11 illustrates graph of acceleration vs. time recorded from impact at the crown with an impact speed of 1.5m/s in the z-axis. Accelerometer shows positive peak acceleration of 699 m/s² (71.3 g). The first negative peak suggests skull flexion experienced by the skull as the skull starts to accelerate. As the skull continues to accelerate there is a significant change in slope of the graph indicated by the peak generated in the positive direction which is the maximum acceleration experienced by the skull in the z-axis followed by another change in the slope of the graph suggesting the deacceleration skull while returning to its original position. Table 3.5 shows acceleration results of the three trials in the z-axis with 1.3 and 1.5m/s impact speeds. The percent difference suggests that the acceleration increases with the increase of the impact speed across the z-axis.

Table 3.5 Z-axis Acceleration Results at Different Impact Speed.

Impact Speed		1.5 m/s	1.3 m/s
Acceleration	Trial 1	699 m/s ² (71.3 g)	642 m/s ² (65.5g)
	Trial 2	660 m/s ² (67.3 g)	632 m/s ² (64.4 g)
	Trial 3	666 m/s ² (67.9 g)	641 m/s ² (65.3 g)
Average		675 m/s ² (68.8 g)	638.3 m/s ² (65.1 g)
Percent Difference		5.6%	

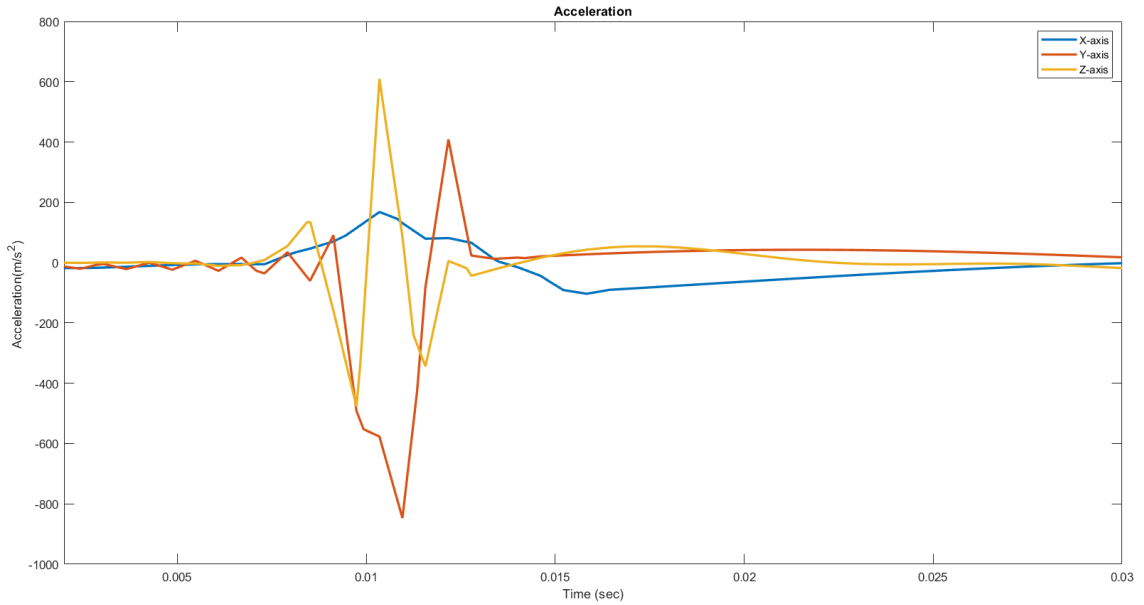


Figure 3.12 Graph of acceleration (m/s^2) vs. time (sec) shows a comparison between all the axis during 1.3m/s impact speed.

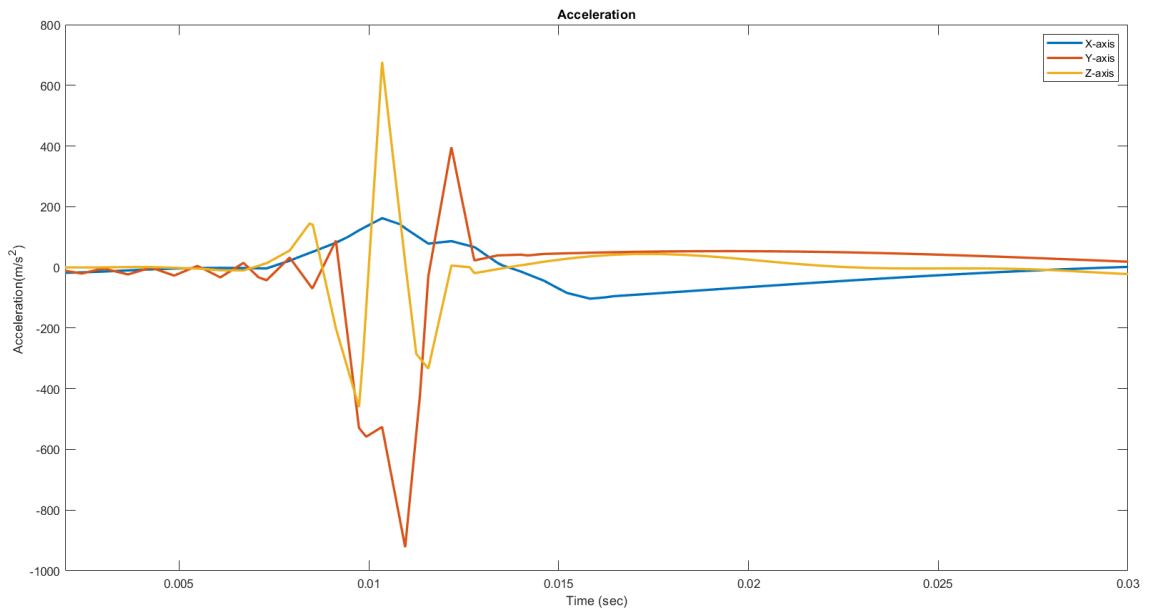


Figure 3.13 Graph of acceleration (m/s^2) vs. time (sec) shows a comparison between all the axis during 1.5m/s impact speed.

Figures 3.12 and 3.13 illustrate a comparison between accelerations across all the axes during the 1.3 and 1.5/s impacts respectively. The graphs shows that the y-axis experience the fastest acceleration, while the x-axis is the least affected by the impact. The graphs also demonstrate that the higher the impact the speed, the higher the acceleration measured meaning the skull is being shaken aggressively at higher impact speeds causing a sever injury to the tissue at the point of impact.

3.4 Angular Rate Sensor Results

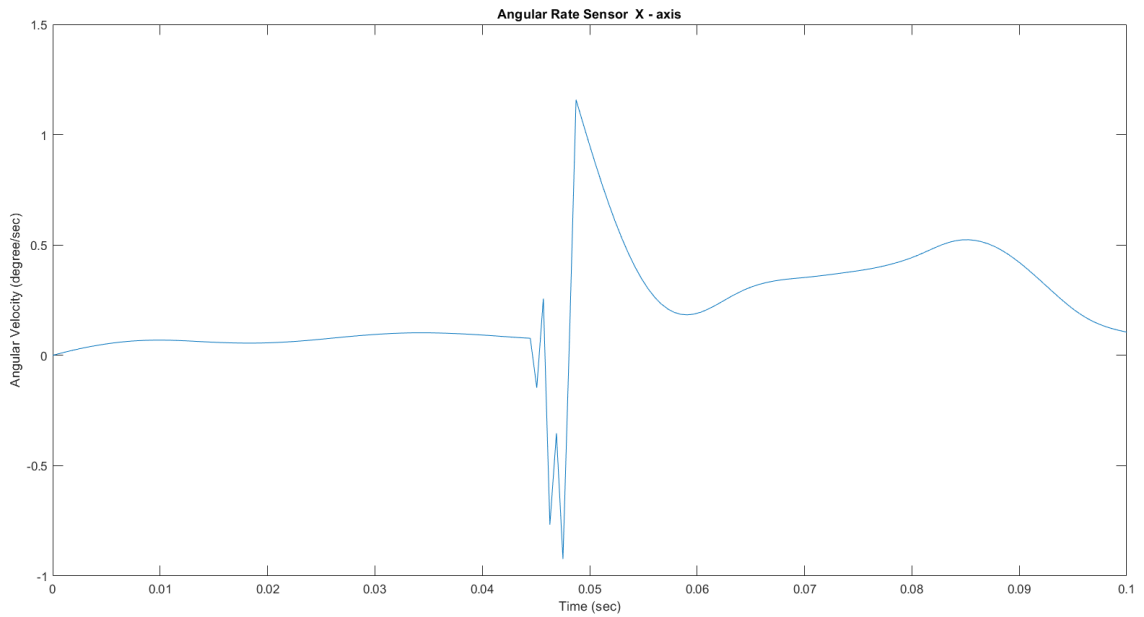


Figure 3.14 Graph of angular velocity (degree/sec) vs. time (sec) shows angular velocity in the X-axis during 1.3m/s impact.

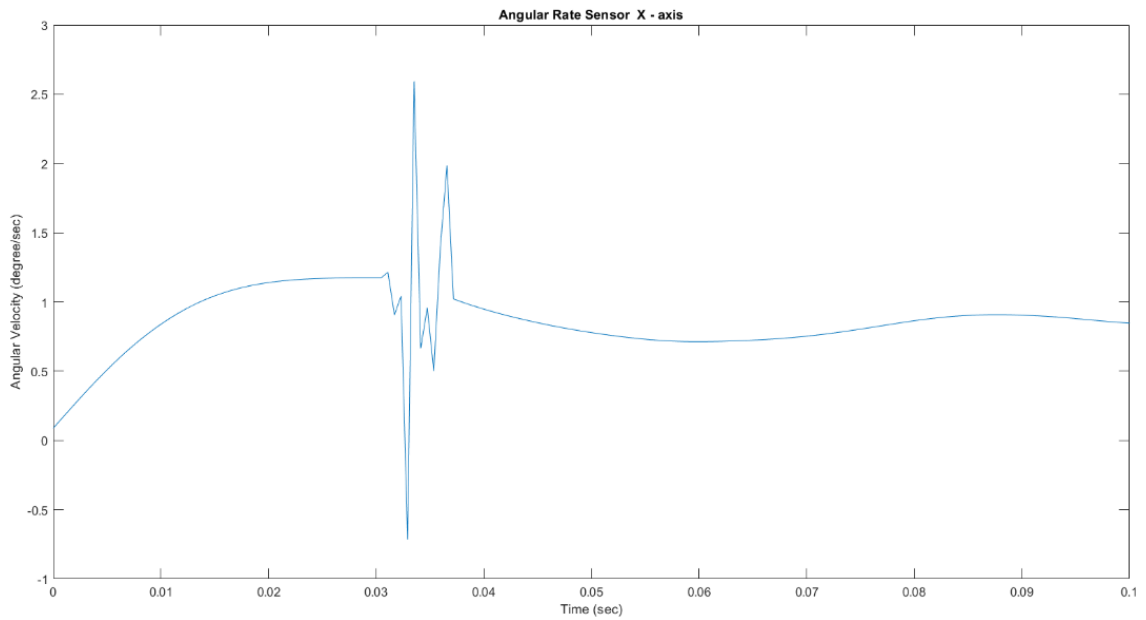


Figure 3.15 Graph of angular velocity (degree/sec) vs. time (sec) shows angular velocity in the X-axis during 1.5m/s impact.

Figure 3.14 illustrates graph of angular velocity vs. time recorded from impact at the crown with an impact speed of 1.3m/s in the x-axis. Accelerometer shows positive peak angular velocity of 1.2 degree/sec. In the beginning of the figure the graph shows negative angular velocity to flexion in the skull, while later the graph shows positive angular velocity.

Figure 3.15 illustrates graph of angular velocity vs. time recorded from impact at the crown with an impact speed of 1.5m/s in the x-axis. Accelerometer shows positive peak angular velocity of 2.6 degree/sec. The first negative peak suggests skull flexion experienced by the skull as the skull starts to accelerate. As the skull continues to accelerate there is a significant change in slope of the graph indicated by the peak generated in the positive direction which is the maximum angular velocity experienced by the skull in the x-axis followed by another change in the slope of the graph suggesting the deceleration/ringing of the skull while returning to its original position. Table 3.6 shows a summary of angular velocity results of the three trials in the x-axis with 1.3 and 1.5m/s impact speeds. The percent difference of in table 3.4 proposes a big difference in angular velocity at the two different impact speeds, while keeping in mind that the impacts resulted in very small angular velocities.

Table 3.6 X-axis Angular Velocity Results at Different Impact Speed.

Impact Speed		1.5 m/s	1.3 m/s
Angular Velocity	Trial 1	2.6 degree/sec	1.2 degree/sec
	Trial 2	2.2 degree/sec	1 degree/sec
	Trial 3	2.4 degree/sec	1.1 degree/sec
Average		2.4 degree/sec	1.1 degree/sec
Percent Difference		74.8%	

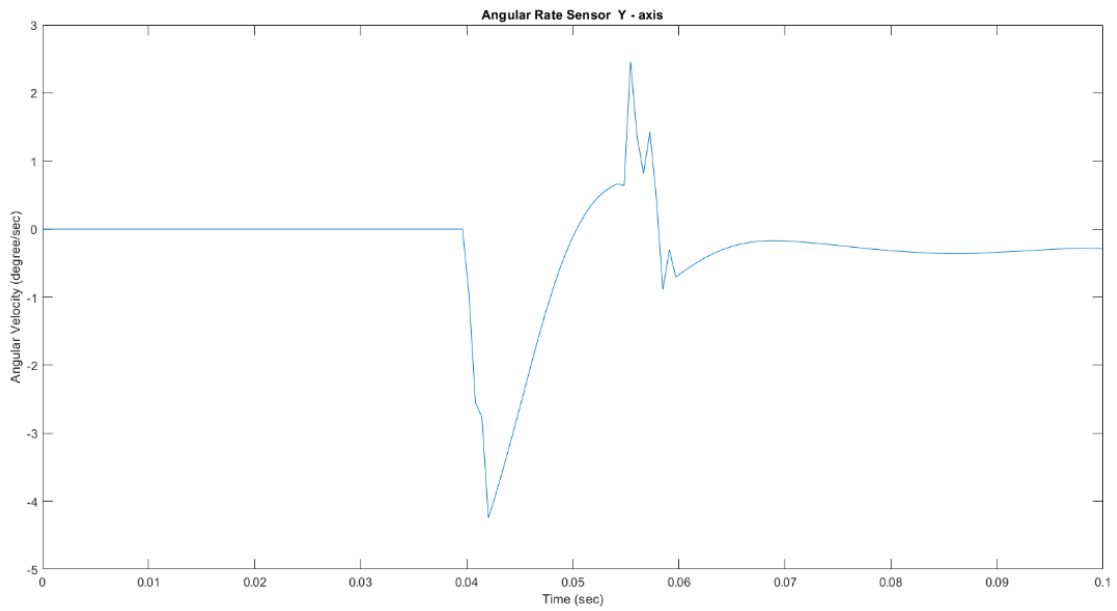


Figure 3.16 Graph of angular velocity (degree/sec) vs. time (sec) shows angular velocity in the Y-axis during 1.3m/s impact.

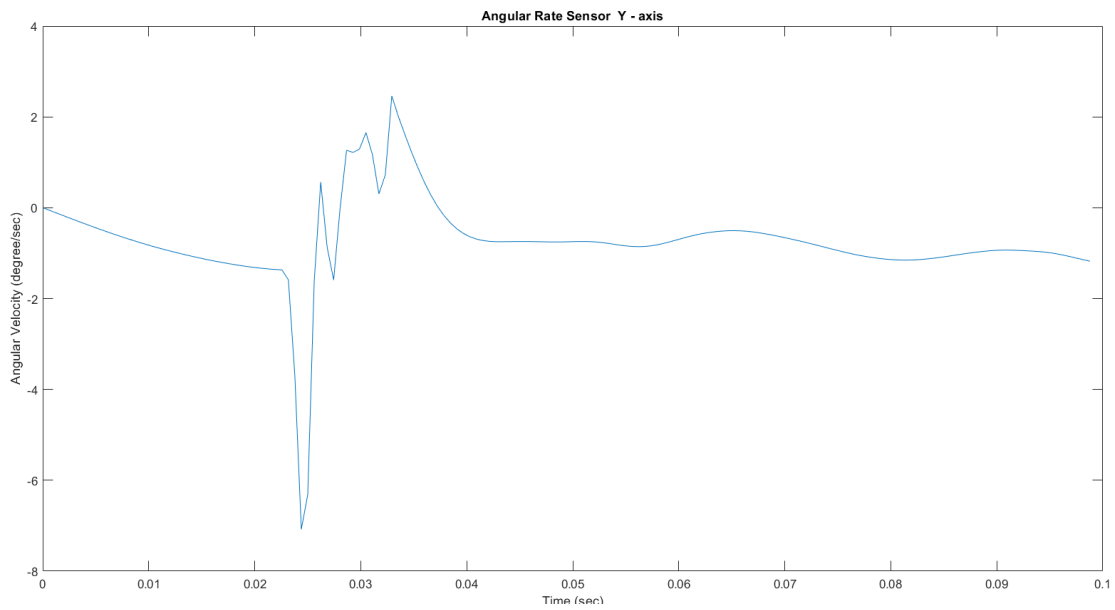


Figure 3.17 Graph of angular velocity (degree/sec) vs. time (sec) shows angular velocity in the Y-axis during 1.5m/s impact.

Figure 3.16 and 3.17 illustrates graph of angular acceleration vs. time recorded from impact at the crown with an impact speed of 1.3 and 1.5 m/s in the y-axis respectively. The graph shows negative peak of angular acceleration of 4.3 and 7 degrees/sec respectively. After the negative peak, the graph shows a positive peak indicating the deacceleration of the skull that is resulting in a positive angular velocity in the y-axis.

Table 3.7 shows a summary of angular velocity results of the three trials in the y-axis with 1.3 and 1.5m/s impact speeds. The percent difference of in table 3.5 suggests a significant change in the angular velocity while decreasing or increasing the impact speed.

Table 3.7 Y-axis Angular Velocity Results at Different Impact Speed.

Impact Speed		1.5m/s	1.3 m/s
Angular Velocity	Trial 1	7 degree/sec	4.3 degree/sec
	Trial 2	6.3 degree/sec	4.1 degree/sec
	Trial 3	6.8 degree/sec	4.2 degree/sec
Average		6.7 degree/sec	4.2 degree/sec
Percent Difference		45.8%	

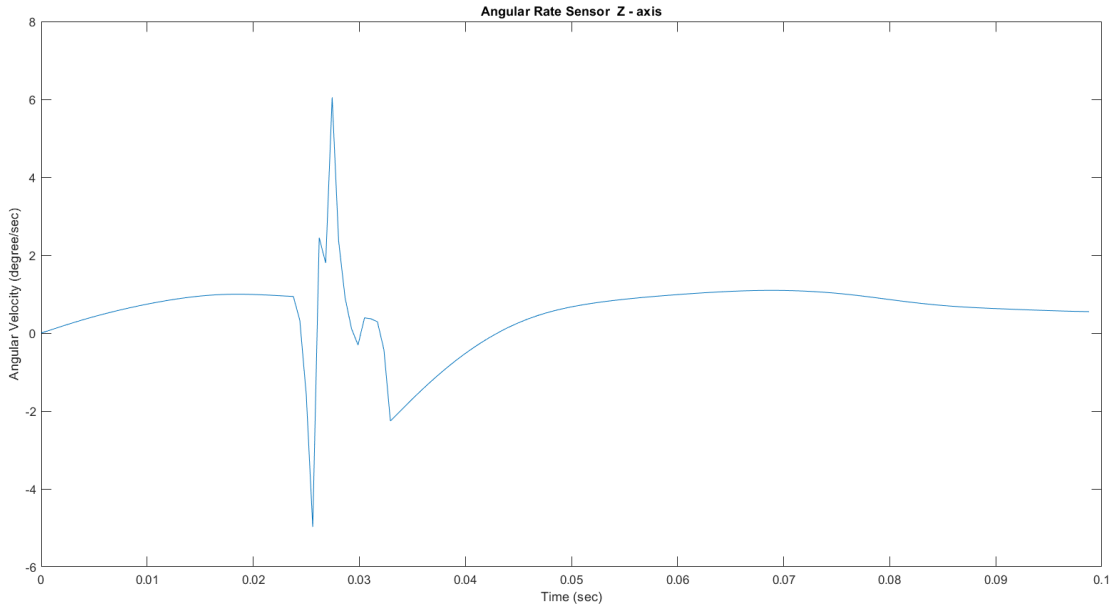


Figure 3.18 Graph of angular velocity (degree/sec) vs. time (sec) shows angular velocity in the Z-axis during 1.3m/s impact.

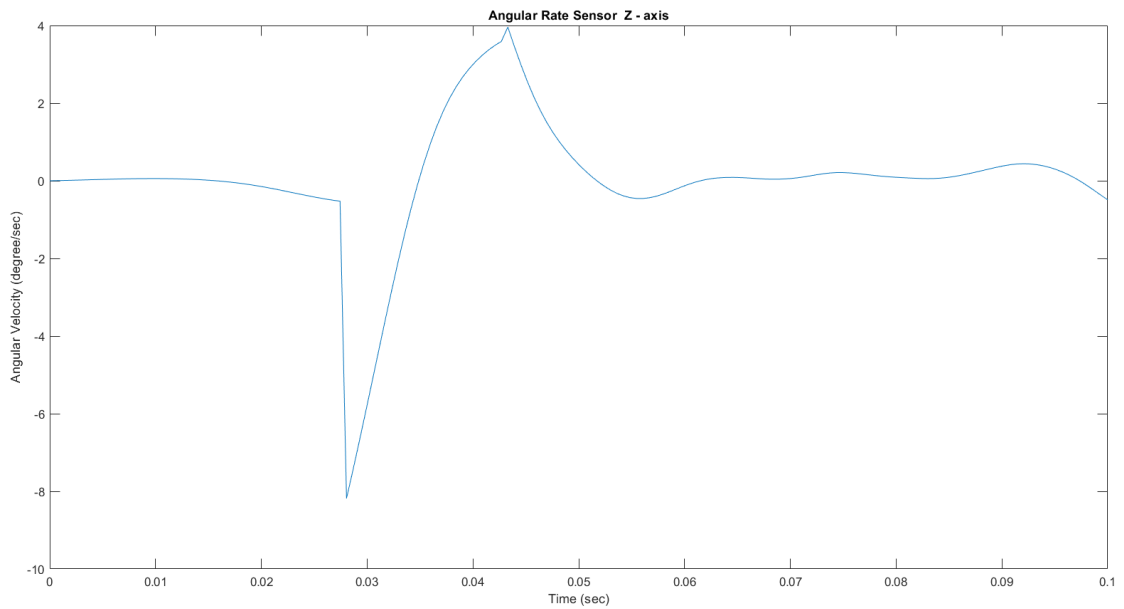


Figure 3.19 Graph of angular velocity (degree/sec) vs. time (sec) shows angular velocity in the Z-axis during 1.5m/s impact.

Figure 3.18 and 3.19 illustrates graph of angular acceleration vs. time recorded from impact at the crown with an impact speed of 1.3 and 1.5 m/s in the z-axis respectively. The graph shows negative peak of angular acceleration of 6 and 8.7 degree/sec respectively.

Table 3.8 shows a summary of angular velocity results of the three trials in the y-axis with 1.3 and 1.5m/s impact speeds. The percent difference of in table 3.6 indicates a significant change in the angular velocity while decreasing or increasing the impact speed.

Table 3.8 Z-axis Angular Velocity Results at Different Impact Speed.

Impact Speed		1.5 m/s	1.3 m/s
Angular Velocity	Trial 1	8.7 degree/sec	6 degree/sec
	Trial 2	8.2 degree/sec	5.7 degree/sec
	Trial 3	8.4 degree/sec	5.8 degree/sec
Average		7.8 degree/sec	5.5 degree/sec
Percent Difference		34.6%	

The figures and tables in sections 3.2 and 3.3 indicate that the higher the impact speed the higher the acceleration and the angular velocity are which means the more severe the injury to head is. For example, in the y-axis the average acceleration trials is -843.2 m/s² and -750.3 m/s² during 1.5 and 1.3 m/s impact speed respectively while the angular velocity is 6.7 and 4.2 degree/sec.

3.5 Strain Gauge Results

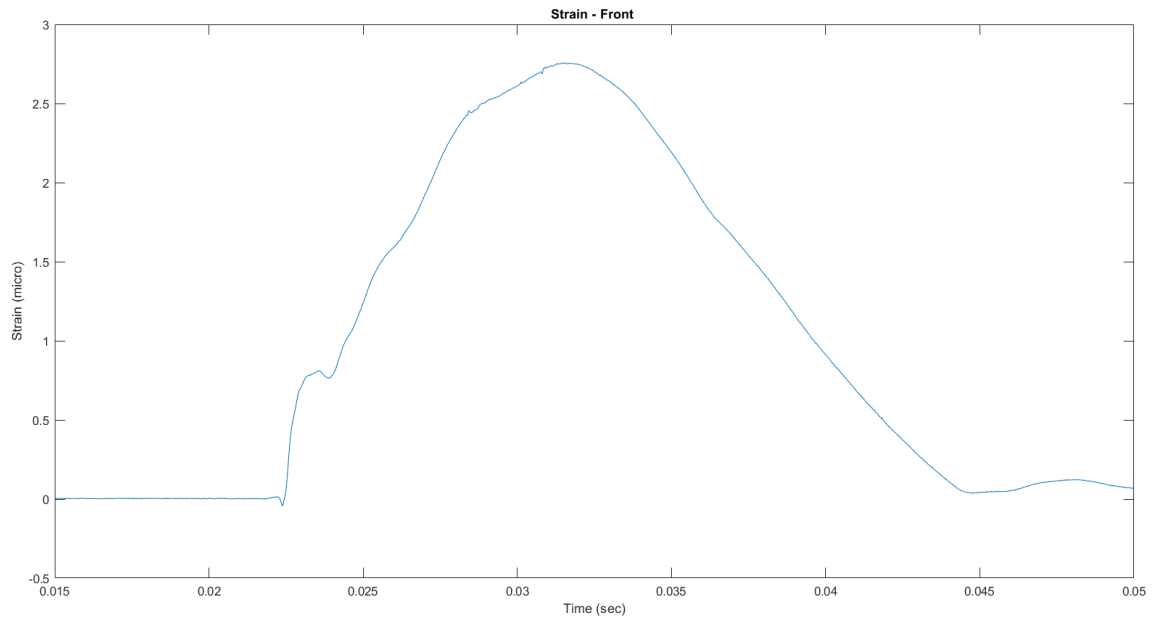


Figure 3.20 Graph of strain vs. time (sec) shows strain in the front of the skull during 1.3m/s impact.

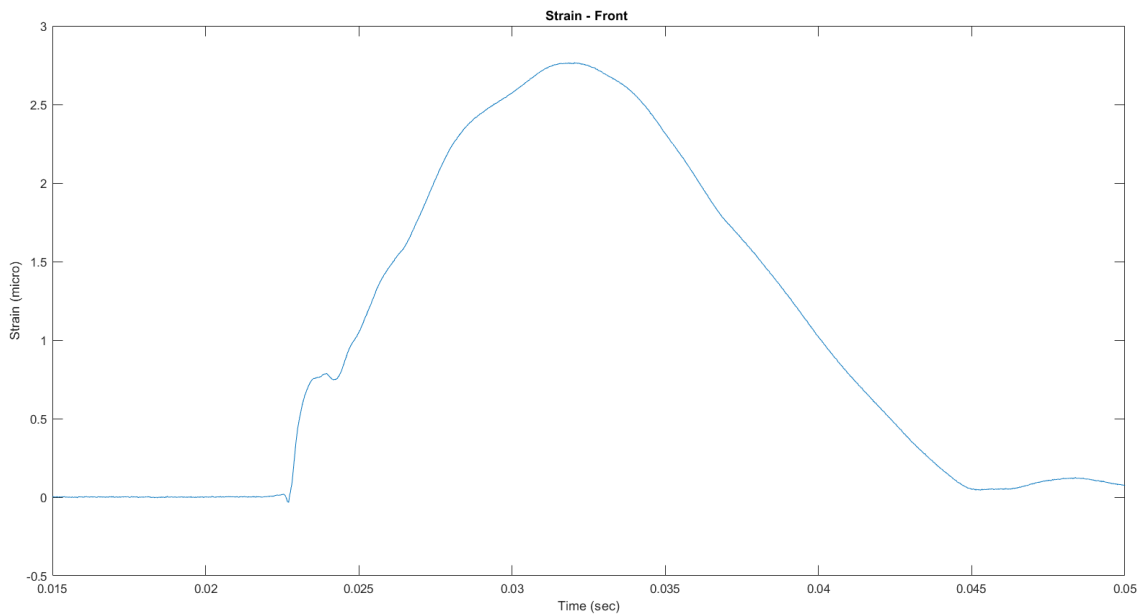


Figure 3.21 Graph of strain vs. time (sec) shows strain in the front of the skull during 1.5m/s impact.

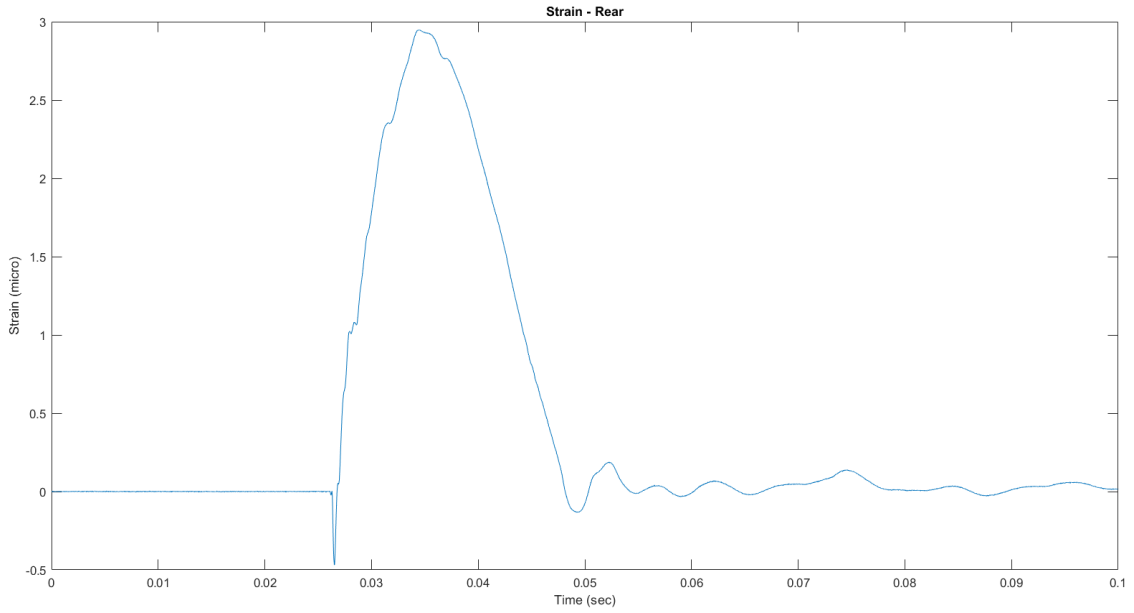


Figure 3.22 Graph of strain vs. time (sec) shows strain in the rear area of the skull during 1.3m/s impact.

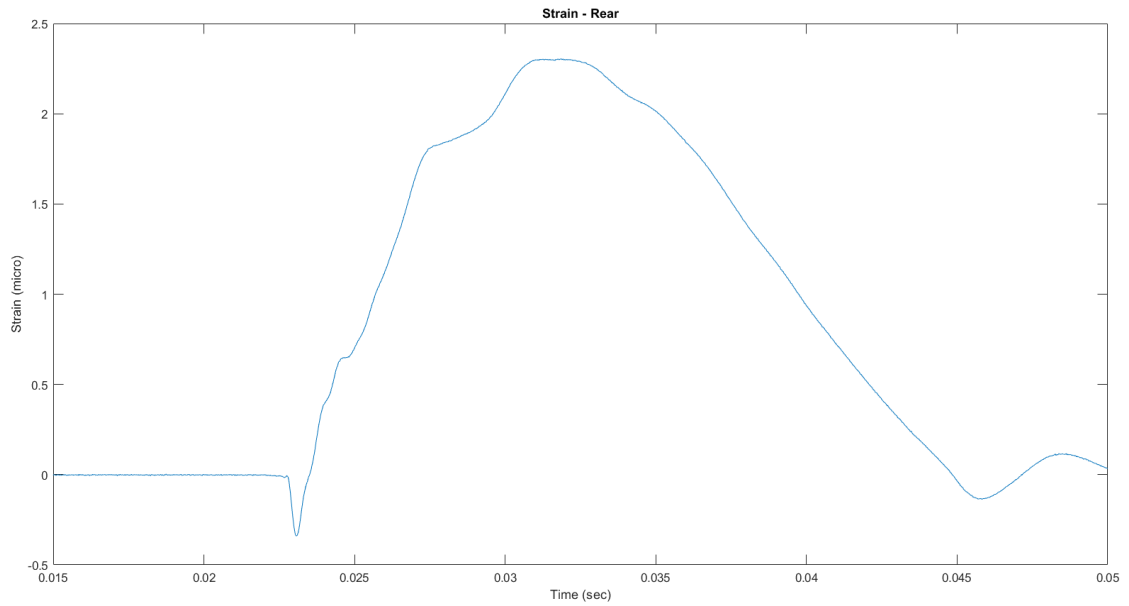


Figure 3.23 Graph of strain vs. time (sec) shows strain in the rear area of the skull during 1.5m/s impact.

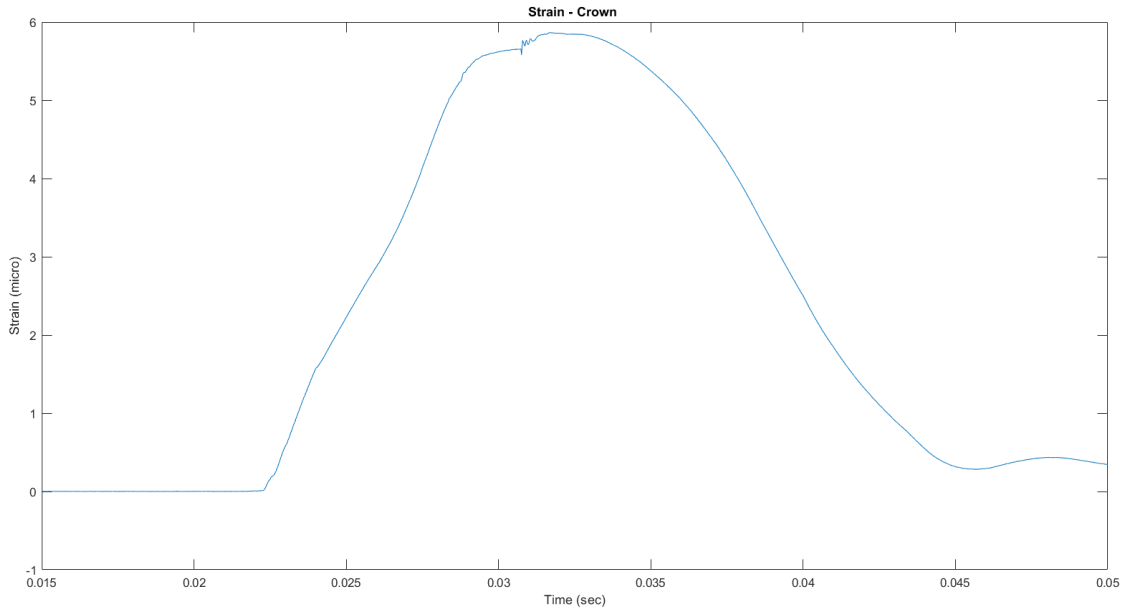


Figure 3.24 Graph of strain vs. time (sec) shows strain in the crown area of the skull during 1.3m/s impact.

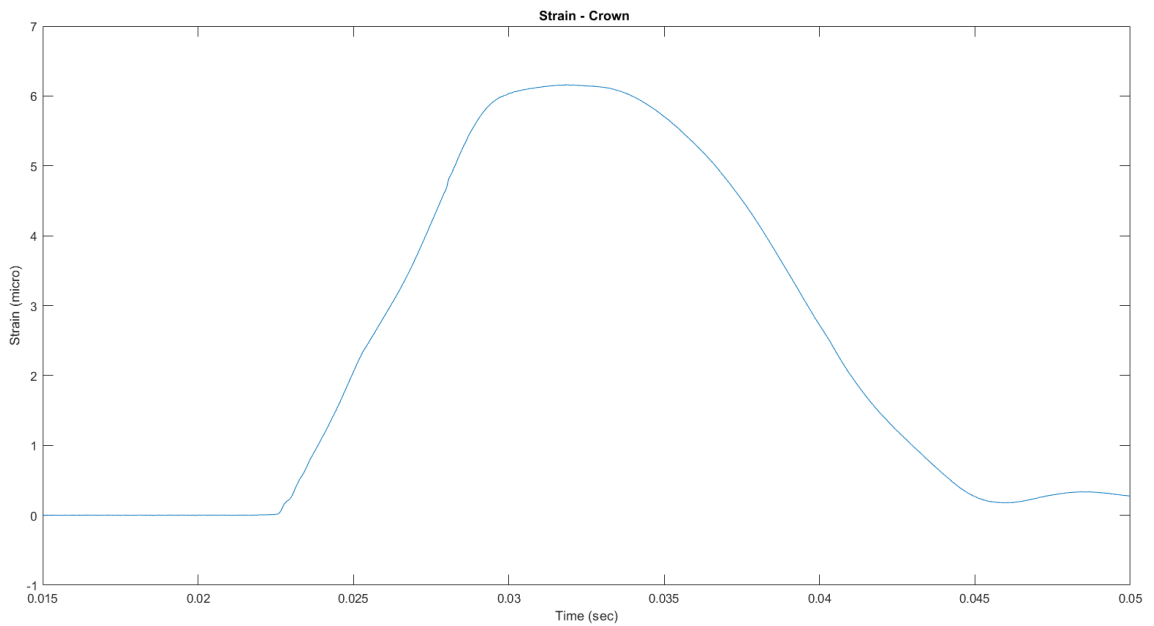


Figure 3.25 Graph of strain vs. time (sec) shows strain in the crown area of the skull during 1.5m/s impact.

Figures 3.20, 3.21, 3.22, 3.23, 3.24 and 3.25 illustrate graph of strain vs time in the crown, front and rear areas of the skull during different impact speeds. Strain gauges show positive values when it stretches, and negative values suggest compression of material. It should be noted that when the projectile makes contact, the slope of the line starts turning positive indicating start of impact. As the skull further continues to deform there is significant change in slope of line indicated by the peak generated which suggest the maximum deformation experienced by the skull. The graphs indicate that the deformation in the skull increase with increasing the impact speed. Tables 3.9, 3.10 and 3.11 show a summary of strain results of the three trials in during 1.3 and 1.5m/s impact speeds.

Table 3.9 Skull Front Results at Different Impact Speed.

Impact Speed		1.5 m/s	1.3 m/s
Strain	Trial 1	2.5 micro	2.5 micro
	Trial 2	2.5 micro	2.4 micro
	Trial 3	2.5 micro	2.4 micro
Average		2.5 micro	2.43 micro
Percent Difference		2.8 %	

Table 3.10 Skull Crown Results at Different Impact Speed.

Impact Speed		1.5 m/s	1.3 m/s
Strain	Trial 1	6.2 micro	5.9 micro
	Trial 2	6.2 micro	5.7 micro
	Trial 3	6.1 micro	5.7 micro
Average		6.2 micro	5.8 micro
Percent Difference		6.7 %	

Table 3.11 Skull Rear Results at Different Impact Speed.

Impact Speed		1.5 m/s	1.3 m/s
Strain	Trial 1	3.0 micro	2.84 micro
	Trial 2	3.0 micro	2.9 micro
	Trial 3	2.9 micro	2.84 micro
Average		2.97 micro	2.86 micro
Percent Difference		3.8 %	

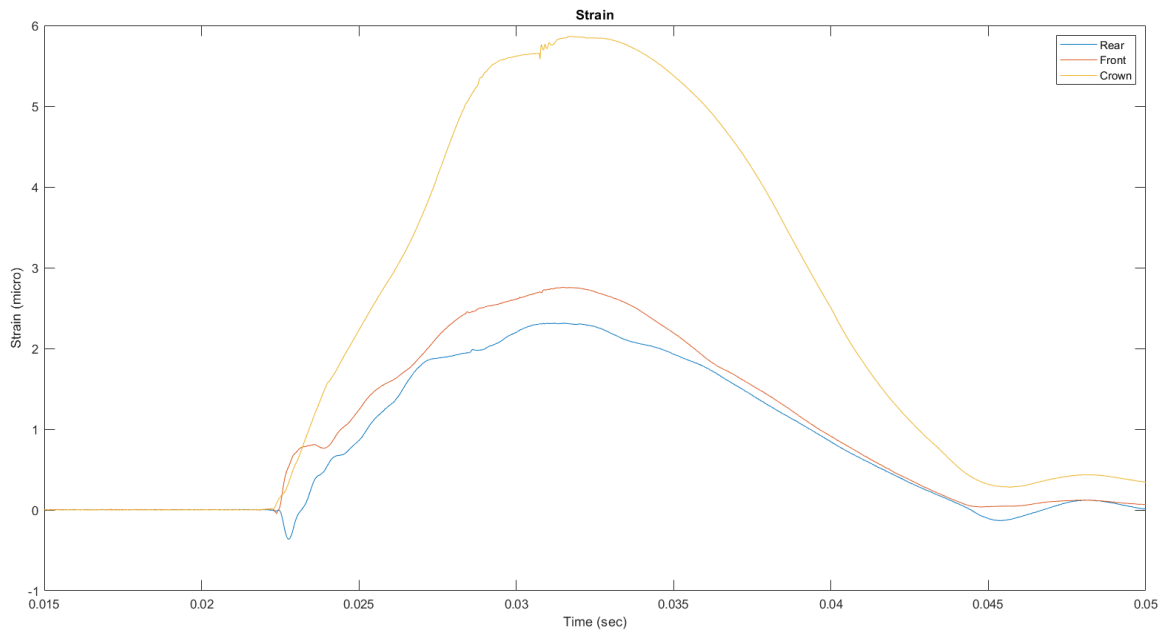


Figure 3.26 Graph of strain vs. time (sec) shows a strain comparison between the front, crown and rear areas of the skull during 1.3m/s impact.

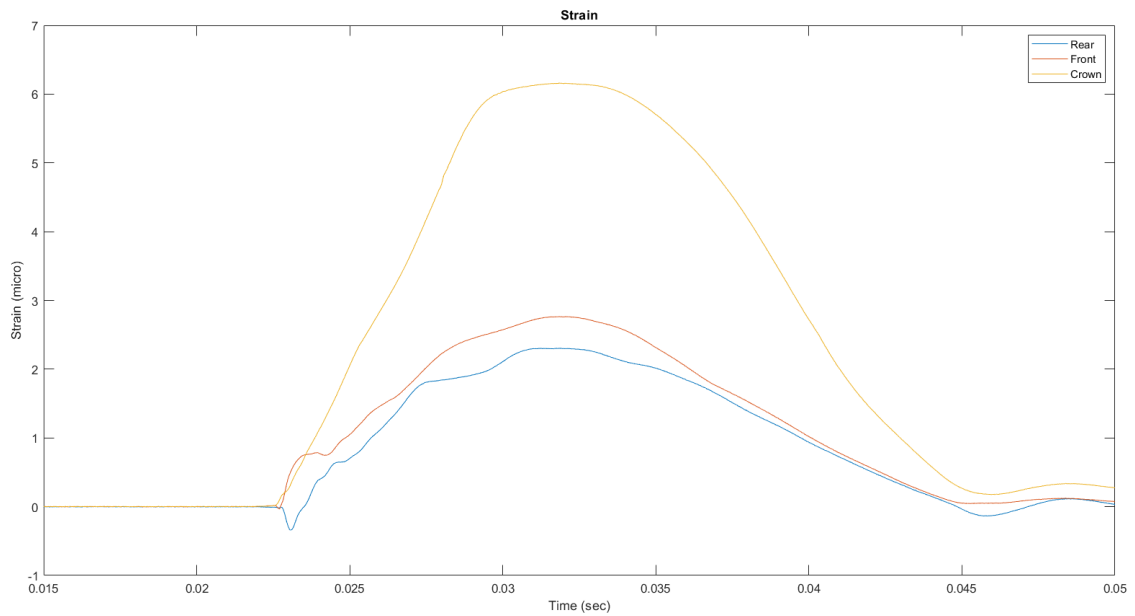


Figure 3.27 Graph of strain vs. time (sec) shows a strain comparison between the front and rear areas of the skull during 1.5m/s impact.

Figures 3.26 and 3.27 shows that the deformation experienced by the crown is higher than those in the front and rear areas of the skull meaning the crown of the skull experienced more tension during the impacts. The graphs also show that rear area undergo the least deformation during the impact.

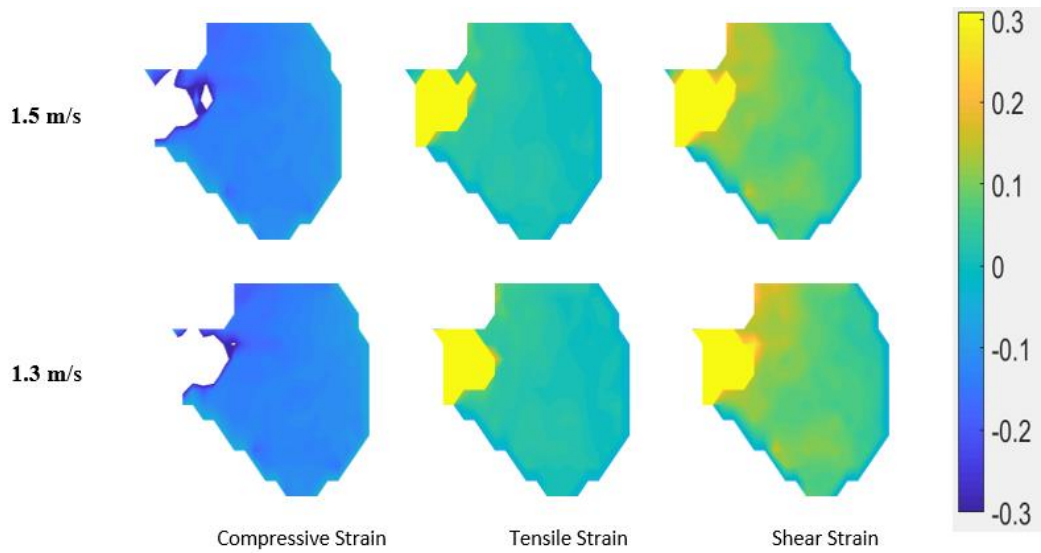


Figure 3.28 Heat maps generated from MATLAB script. Rows top to bottom represent the impact speed. The columns from left to right represent the type of strain experienced. The intensity of the strain is explained with the help bar graph.

Figure 3.28 illustrates heat maps of brain surrogate deformation pattern. Compression and shear stress are more concentrated in the left of the crown area down to the base of the skull. The reason behind noticing a shear stress in the jaw area is because the skull is mounted on a rectangular polycarbonate plate with jaw line parallel to the plate. In general, there is no significant difference between the heat maps of the brain at the two different impact speeds.

3.6 HIC

As discussed previously the center of gravity of the skull model was projected to the surface of the model for the ease of measuring the acceleration of an inaccessible point within the rigid body. The three accelerometers were used to measure directly the acceleration at each axis while the angular rate sensors were used to measure the angular velocity at each axis. Below are the results for the equations listed in section 2.2

During an impact speed of 1.5 m/s:

$$A_{0x} = A_{1X} + r_x (w_y^2 + w_z^2) = 155.9 + 0.07 (6.3^2 + 7.8^2) = 162.9 \text{ m/s}^2 (16.6 \text{ g})$$

$$A_{0y} = A_{2y} + r_y (w_x^2 + w_z^2) = -843.2 + 0.07 (2.2^2 + 7.8^2) = -839.3 \text{ m/s}^2 (-85.5 \text{ g})$$

$$A_{0z} = A_{3z} + r_z (w_x^2 + w_y^2) = 675 + 0.1 (2.2^2 + 6.3^2) = 679.5 \text{ m/s}^2 (69.3 \text{ g})$$

During an impact speed of 1.3 m/s:

$$A_{0x} = A_{1X} + r_x (w_y^2 + w_z^2) = 155.7 + 0.07 (4.1^2 + 5.5^2) = 159.0 \text{ m/s}^2 (16.2 \text{ g})$$

$$A_{0y} = A_{2y} + r_y (w_x^2 + w_z^2) = -750.3 + 0.07 (1^2 + 5.5^2) = -748.1 \text{ m/s}^2 (-76.3 \text{ g})$$

$$A_{0z} = A_{3z} + r_z (w_x^2 + w_y^2) = 638.3 + 0.1 (1^2 + 4.1^2) = 640.1 \text{ m/s}^2 (65.3 \text{ g})$$

Head Injury Criteria is calculated at the resultant linear acceleration measured at the center of gravity integrated over 15ms which is the duration of the injury where the highest HIC values is generated. The equation is listed in section 1.3.

During an Impact speed of 1.5 m/s:

$$\text{HIC} = \left[\frac{1}{0.02-0.0185} \int_{0.0185}^{0.02} 111 dx \right]^{2.5} (0.02 - 0.0185) = 195g$$

During an Impact speed of 1.3 m/s:

$$\text{HIC} = \left[\frac{1}{0.02-0.0185} \int_{0.0185}^{0.02} 101 dx \right]^{2.5} (0.02 - 0.0185) = 153g$$

To validate the measured acceleration at the center of gravity(CG), a dot was placed in the center of gravity of the skull and tracked using ProAnalyst software. Since the software can only track a mark in a 2D plane, then CG acceleration was tracked as two components and the resultant linear acceleration at the CG was calculated. That, the measured resultant CG from ProAnalyst software was compared with the measured resultant linear acceleration from LabVIEW. The 2D tracked mark data was exported from ProAnalyst as displacement measurements in an excel spreadsheet. The spreadsheet was loaded into MATLAB and differentiated to obtain velocity and acceleration data. The acceleration measurements from LabVIEW were loaded into MATLAB and filtered. Table 3.12 summarizes the difference between the two measured data, and HIC was calculated. The instrumented device proves again that it is measurements are validated, since the measured data within 8% error which acceptable.

Table 3.12 HIC Results at Different Impact Speed.

Impact Speed	Axis	ProAnalyst	Experimental	Percent Difference
1.5m/s	Y	-86g (-845 m/s ²)	-85g (-839 m/s ²)	1%
	Z	64g (637 m/s ²)	69g (679 m/s ²)	7%
	Resultant	107g	110g	2.8%
	HIC	179	191	6%
1.3m/s	Y	-74g (727 m/s ²)	-76g (748 m/s ²)	3%
	Z	63g (620 m/s ²)	65g (640 m/s ²)	3%
	Resultant	97g	100g	3%
	HIC	139	150	8%

CHAPTER 4

CONCLUSION AND FUTURE SCOPE

This thesis builds on previous work, using the same head models. Some questions mentioned in Bhatambarekar 2017 remained unexplored. The skull kinematics such as acceleration and deceleration of the skull, angular velocity and angular acceleration are very important factor in injury assessment. The skull- brain surrogate model used here was 3D printed ABS half skull. The geometry of the skull reflects the geometry of the real human skull. The brain surrogate used here is 20% ballistic gel which is commonly used. The skull-brain surrogate was experimented on a drop tower apparatus at 1.3 and 1.5 m/s impact speed.

The purpose of this study was to evaluate an instrumented device as a research device for measuring head impact kinematics and link it to brain deformation. the instrumented device included direct six degree of freedom measurements of head movement and rotation; 3 degree of freedom as linear acceleration and 3 degree of freedom as angular velocity. In this thesis only accelerometers, angular rate sensors and strain gauges were used to measure acceleration, angular velocity and skull deformation respectively. Using three accelerometers and three angular rate sensors allowed us to measure acceleration and angular velocity directly and relate those measurement to the center of the gravity of the skull model at different impact speeds.

An initial experiments was carried out to validate the ADXL377 accelerometer measurements (section 3.1). The results of this experiment state that the ADXL377 measurement are validated within 5% error which is acceptable. Next, another experiment was performed to compare a costly accelerometer (Endevco 7264) and an

inexpensive accelerometer(ADXL377) (section 3.2). The results of this experiment expressed that the accelerometers measurements are within 3% which demonstrates that an accurate results can be obtained with an economical sensors as well as pricey ones. After the second experiment, it was decided that the rest of experiments will be performed using ADXL377 accelerometer.

Later, six experiments were conducted with an impact speed of 1.3 and 1.5m/s (three experiments at each impact speed) using the strain gauges, accelerometers, and angular rate sensors. Skull deformation was calculated using strain gauges (section 3.4) and it was noticed that the deformation experienced by the crown is higher than those in the front and rear areas of the skull meaning the crown of the skull experienced more tension during the impacts. Brain deformation strains were calculated and it was observed that the crown and the jaw experienced the most shear stress at a higher impact speed.

Using the accelerometer and angular rate measurement, peak linear acceleration was calculated and related to the center of gravity acceleration, and the resultant linear acceleration at the center of gravity was calculated. The resultant CG acceleration measurements exported from LabVIEW were compared to the resultant linear acceleration that was obtained by the high-speed video camera. The percent error between the camera and experimental measurements of the linear acceleration at the center of gravity was within 3% which is negligible. After comparing the linear acceleration at the center of gravity, head injury criteria was calculated by integrating the resultant over a 15 ms period of time and compared for both camera and experimental measurements. The percent difference of HIC was below 8%.

The calculated percent difference in the study is generally below 8% which indicates that the instrumented device is very reliable and that it meets the design requirements and can be used in further experiments. The design requirements were met when the device measured skull's linear acceleration, angular velocity and strain. The linear acceleration and angular velocity were then analyzed and evaluated. The strain gauges were used to measure skull strain and brain strain were calculated and linked to head kinematics.

In conclusion, in this work, an instrumented device is presented to measure head kinematics during an impact. Laboratory testing demonstrated the efficacy of measuring peak values and of linear acceleration, angular acceleration, and angular velocity. The instrumented device can potentially be used in the case of acceleration based injuries such as motor vehicle crashes, where understanding the rupture of veins between the skull and the brain is a major concern. In other words, this economical instrumented model can measure the relative motion of the skull and brain deformation models to be compared to real world case studies.

APPENDIX A

STRAIN GAGE VALIDATION EXPERIMENT

This experiment was conducted by Prasad Bhatambarekar to validate the strain gage measurements. A cantilever beam was loaded with three different weights at the free end. The strain gages were mounted axially on the top and the bottom to measure the tension and compression. Theoretical calculation and practical results were with 2% error which is negligible.

The following parameter were used to perform the test:

Material of cantilever beam: Brass 11 [15]

$$F = m * a \text{ (Eq.1)}$$

$$M = F * L \text{ (Eq.2)}$$

$$I = (b * h^3) / 12 \text{ (Eq.3)}$$

$$\epsilon = (M * h) / (2 * E * I) \text{ (Eq.4)}$$

The variables used for equation 1 through 4 are as follows, by order of arrangement: F, force; m, mass; a, acceleration due to gravity; M, moment of force; L, length of beam; I, moment of inertia; b, width of beam; h, thickness of beam; ϵ , engineering strain; E, modulus of elasticity.

Table A.1 Cantilever Beam Properties [8]

Variable	Value
Modulus of Elasticity, E	100 GPa
Mass, m	4.74 kg
Acceleration due to gravity, a	9.81 m/s ²
Length of beam, L	0.15 m
Width of beam, b	0.009 m

Table A.2 Theoretical Calculation of Cantilever Beam Experiment Along with Practical Value of Strain Recorded Using Strain Gauge

Parameter	Value
Force (Eq.1)	46.56 m/s
Moment (Eq.2)	14.19 N-m
Inertia (Eq.3)	5.46 E-10 m ⁴
Strain (Eq.4)	1.168 microstrain
Experimental value of strain	0.789 microstrain

APPENDIX B

MATLAB SCRIPT 1

The following MATLAB script was developed to be used to analyze linear acceleration, angular velocity and strain. Green color suggest notes meant for explanation or description of the function being carried out.

```
%%%%%%%%%%%%%%%%%%%%%%%%%%%%%%%%%%%%%%%%%%%%%%%%%%%%%%%%%%%%%%%%%%%%%%%%  
%%%%%%%%%%%%%%%%%%%%%%%%%%%%%%%%%%%%%%%%%%%%%%%%%%%%%%%%%%%%%%%%%%%%%%%% Linear Acceleration %%%%%%%%%  
%%%%%%%%%%%%%%%%%%%%%%%%%%%%%%%%%%%%%%%%%%%%%%%%%%%%%%%%%%%%%%%%%%%%%%%%
```

```
Fs = 1650; % Sampling frequency
```

```
%%%%%%%%%%%%%%%%%%%%%%%%%%%%%%%%%%%%%%%%%%%%%%%%%%%%%%%%%%%%%%%%%%%%%%%%  
%%%%%%%%%%%%%%%%%%%%%%%%%%%%%%%%%%%%%%%%%%%%%%%%%%%%%%%%%%%%%%%%%%%%%%%% Z- Axis %%%%%%%%%  
%%%%%%%%%%%%%%%%%%%%%%%%%%%%%%%%%%%%%%%%%%%%%%%%%%%%%%%%%%%%%%%%%%%%%%%%
```

```
Z2 = Z-1.5;  
Z3 = Z2 .* 153.8;  
Z4 = Z3 .* 9.8;  
Z5 = Z4 -Z4(1);  
Z6 =Z5 ([69:300]);
```

```
[B,A] = butter (2,500/Fs,'high');  
Z_high = filtfilt(B,A,Z6_1);
```

```
%Filter our 60Hz  
[B60,A60] = butter (4,[59/Fs 61/Fs], 'stop');  
Z6_notch= filtfilt(B60,A60, Z6_2);
```

```
%Low Pass Filter  
[B,A] = butter (4, 200/Fs,'low');  
Z_6 = filtfilt (B,A,Z6_notch);  
Z7 = [Z_high;Z_6];  
t_accel_Z = linspace(0,length(Z7)/Fs,length(Z7)); % Creates time vector for acceleration
```

```
% intergrating acceleration to velocity  
Velocity_Z = cumtrapz(t_accel_Z, Z7);  
t_velocity_Z = linspace(0,length(Velocity_Z)/Fs,length(Velocity_Z));
```

```

%% intergrating velocity to distance
Distance_Z = cumtrapz(t_velocity_Z, Velocity_Z);
t_distance_Z = linspace(0,length(Distance_Z)/Fs,length(Distance_Z)); % Creates time
vector

%plotting acceleration, velocity, distance in Z-axis
figure (1)
%subplot(3,1,1)
csZ = csapi(t_accel_Z, -Z7);
fnplt(csZ,2);
%plot (t_accel_Z ,Z7, 'b')
title ('Acceleration Z - axis')
xlabel('Time (sec)')
ylabel('Acceleration(m/s^2) ')
xlim ([0 0.05])
%
% figure(2)
% plot(t_velocity_Z, (Velocity_Z),'b')
% title ('Velocity Z - axis')
% xlabel('Time (sec)')
% ylabel('Velocity (m/s)')
%
% figure(3)
% plot(t_distance_Z, -(Distance_Z),'g')
% title ('Distance Z - axis')
% xlabel('Time (sec)')
% ylabel('Distance (m)')
% xlim ([0 0.05])
% %
%
% % % % % % % % % % % % % % % % % %
% % % % % Y- Axis % % % % %
% % % % % % % % % % % % % % % % % %
%
Fs = 1650;
Y2 = -Y-1.5;
Y3 = Y2 .* 153.8;
Y4 = Y3 .* 9.8;
Y5 = Y4 -Y4(1);
Y6 = Y5 ([70: 110]);
Y6_1 = Y5 ([70:88]);

Y6_2 = Y5 ([89:110]);
%

```

```

% [B,A] = butter (2,50/Fs,'high');
% Y_high = filtfilt(B,A,Y6_1);

% %Filter our 60Hz
% [B60,A60] = butter (4,[59/Fs 61/Fs], 'stop');
% Y6_notch= filtfilt(B60,A60, Y6_2);

%Low Pass Filter
[B,A] = butter (4,200/Fs,'low');
Y_low = filtfilt (B,A,Y6_2);

Y7 = [Y6_1;Y_low];
t_accel_Y = linspace(0,length(Y7)/Fs,length(Y7)); % Creates time vector for
acceleration

%% intergrating acceleration to velocity
Velocity_Y = cumtrapz(t_accel_Y, Y7);
t_velocity_Y = linspace(0,length(Velocity_Y)/Fs,length(Velocity_Y));

%% intergrating velocity to distance
Distance_Y = cumtrapz(t_velocity_Y, Velocity_Y);
t_distance_Y = linspace(0,length(Distance_Y)/Fs,length(Distance_Y)); % Creates time
vector

%plotting acceleration, velocity, distance in Z-axis
figure (4)
csY = csapi(t_accel_Y, Y7-Y7(1));
fnplt(csY,2);
plot (t_accel_Y, Y7, 'b')
title ('Acceleration Y - axis')
xlabel('Time (sec)')
ylabel('Acceleration(m/s^2) ')
xlim ([0 0.025])
%
%
% figure(5)
% plot(t_velocity_Y, (Velocity_Y),'b')
% title ('Velocity Y - axis')
% xlabel('Time (sec)')
% ylabel('Velocity (m/s)')
%
% figure(6)
% plot(t_distance_Y, (Distance_Y),'g')
% title ('Distance Y - axis')

```



```

% xlabel('Time (sec)')
% ylabel('Distance (m)')
%
%
% %%%%%%%%%%
% %%%%%%%%% X- Axis %%%%%%%%%
% %%%%%%%%%%
%
Fs = 1650;
X2 = -X-1.5;
X3 = X2 .* 153.8;
X4 = X3 .* 9.8;
X5 = X4 -X4(1);
X6 = X5 ([80: 305]);

X6_1 = X5 ([96:109]);
X6_3 = X5 ([83: 95]);
X6_2 = X5 ([110:305]);

[B,A] = butter (2, 150/Fs,'low');
X_high = filtfilt(B,A,X6_3);

%Filter our 60Hz
[B60,A60] = butter (4,[59/Fs 61/Fs], 'stop');
X6_notch= filtfilt(B60,A60, X6_2);

%Low Pass Filter
[B,A] = butter (4, 50/Fs,'low');
X_low = filtfilt (B,A,X6_notch);

X7 = [X_high;X6_1;X_low];
% X7 = X7([0.005:0.05
t_accel_X = linspace(0,length(X7)/Fs,length(X7)); % Creates time vector for
acceleration

% t_accel_X = linspace(0,length(X6)/Fs,length(X6)); % Creates time vector for
acceleration
%
% %%% intergrating acceleration to velocity
% Velocity_X = cumtrapz(t_accel_X, X6);
% t_velocity_X = linspace(0,length(Velocity_X)/Fs,length(Velocity_X));
%
% %%% intergrating velocity to distance
% Distance_X = cumtrapz(t_velocity_X, Velocity_X);

```

```

% t_distance_X = linspace(0,length(Distance_X)/Fs,length(Distance_X)); % Creates time
vector
%
%
%plotting acceleration, velocity, distance in Z-axis
figure (7)
%subplot(3,1,1)
csX = csapi(t_accel_X, X7);
fnplt(csX,2);
%plot (t_accel_X ,X6, 'b')
title ('Acceleration X - axis')
xlabel('Time (sec)')
ylabel('Acceleration(m/s^2) ')
xlim ([0 0.05])

% figure(8)
% plot(t_velocity_X, (Velocity_X),'b')
% title ('Velocity X - axis')
% xlabel('Time (sec)')
% ylabel('Velocity (m/s)')
%
% figure(9)
% plot(t_distance_X, (Distance_X),'g')
% title ('Distance X - axis')
% xlabel('Time (sec)')
% ylabel('Distance (m)')

figure (17)
fnplt(csX,2);
hold on
fnplt(csY,2);
hold on
fnplt(csZ,2);
title ('Acceleration')
xlabel('Time (sec)')
ylabel('Acceleration(m/s^2) ')
xlim ([0.002 0.03])
legend('X-axis', 'Y-axis', 'Z-axis')

%%%%%%%%%%%%%%
%%%%%%%%%%%%%% Angular Velocity %%%%%%%%%%%%%%%
%%%%%%%%%%%%%%

%%%%%%%%%%%%%%

```

```

%%%%%%%%% X- Axis %%%%%%%%%
%%%%%%%%%

Fs = 1650;
Y_rot = Xrot - Xrot(1);
Y_rot_1 = Y_rot .* 10576.4;

[B60,A60] = butter (2,[59/Fs 61/Fs], 'stop');
Y_rot_2 = filtfilt(B60,A60,Y_rot_1);

Y_rot2 = Y_rot_2 ([96:105]);

%first section
Y_rot_4 = Y_rot_2 ([45:95])
[B,A] = butter (2,50/Fs,'low');
Y_rot_4_low = filtfilt(B,A, Y_rot_4);

%Low Pass Filter third section
Y_rot_3 = Y_rot_2 ([93:200]);
[B,A] = butter (2, 50/Fs,'low');
Y_low = filtfilt (B,A,Y_rot_3);

Y3 = [Y_rot_4_low;Y_rot2; Y_low]
t_distance_X = linspace(0,length(Y3)/Fs,length(Y3)); % Creates time vector

figure(10)
plot ( t_distance_X, Y3)
title('Angular Rate Sensor X - axis')
xlabel('Time (sec)')
ylabel('Angular Velocity (degree/sec)')

%%%%%%%%%
%%%%%%%%% Z- Axis %%%%%%%%%
%%%%%%%%%

%
Fs = 1650;
Z_rot = Zrot - Zrot(1);
Z_rot_1 = Z_rot .* 10576.4;

[B60,A60] = butter (2,[59/Fs 61/Fs], 'stop');
Z_rot_2 = filtfilt(B60,A60,Z_rot_1);

Z_rot2 = Z_rot_2 ([78:91]);

%first section

```

```

Z_rot_4 = Z_rot_2 ([38:77])
[B,A] = butter (2,50/Fs,'low');
Z_rot_4_low = filtfilt(B,A, Z_rot_4);

%Low Pass Filter third section
Z_rot_3 =Z_rot_2 ([92:200]);
[B,A] = butter (2, 50/Fs,'low');
Z_low = filtfilt (B,A,Z_rot_3);

Z3 = [Z_rot_4_low;Z_rot2; Z_low]
t_distance_Z = linspace(0,length(Z3)/Fs,length(Z3)); % Creates time vector

figure(11)
plot ( t_distance_Z, Z3-Z3(1))
title('Angular Rate Sensor Z - axis')
xlabel('Time (sec)')
ylabel('Angular Velocity (degree/sec)')

%%%%%%%%%%%%%
%%%%%%%%% Y- Axis %%%%%%%%%
%%%%%%%%%%%%%

Fs = 1650;
Y_rot = Yrot - Yrot(1);
Y_rot_1 = Y_rot .* 10576.4;

[B60,A60] = butter (2,[59/Fs 61/Fs], 'stop');
Y_rot_2 = filtfilt(B60,A60,Y_rot_1);

Y_rot2 = Y_rot_2 ([78:80]);
Y_rot2A = Y_rot_2 ([101:108]);

Y_rot_5 = Y_rot_2 ([81:101]);
[B,A] = butter (2,100/Fs,'low');
Y_rot_2_low = filtfilt(B,A, Y_rot_5);

%first section
Y_rot_4 = Y_rot_2 ([10:75])
[B,A] = butter (2,1/Fs,'low');
Y_rot_4_low = filtfilt(B,A, Y_rot_4);

%Low Pass Filter third section
Y_rot_3 = Y_rot_2 ([109:200]);
[B,A] = butter (2, 60/Fs,'low');
Y_low = filtfilt (B,A,Y_rot_3);

```

```

Y3 = [Y_rot_4_low;Y_rot2;Y_rot_2_low;Y_rot2A; Y_low]
t_distance_Y = linspace(0,length(Y3)/Fs,length(Y3)); % Creates time vector

figure(12)
plot ( t_distance_Y, Y3-Y3(1))
% hold on
% plot (Y_rot_1)
title('Angular Rate Sensor Y - axis')
xlabel('Time (sec)')
ylabel('Angular Velocity (degree/sec)')
xlim ([0 0.1])

%%%%%%%%%%%%%%%%%%%%%%%%%%%%%%%%%%%%%%%%%%%%%%%%%%%%%%%%%%%%%%%%%%%%%%%%
%%%%%%%%%%%%%%%%%%%%%%%%%%%%%%%%%%%%%%%%%%%%%%%%%%%%%%%%%%%%%%%%%%%%%%%% Strain Gage %%%%%%%%%
%%%%%%%%%%%%%%%%%%%%%%%%%%%%%%%%%%%%%%%%%%%%%%%%%%%%%%%%%%%%%%%%%%%%%%%%

Fs= 50000;
Rear2 = (Rear - Rear(1)) .*(1000);
t_distance_R = linspace(0,length(Rear2)/Fs,length(Rear2)); % Creates time vector
figure (13)
plot ( t_distance_R, Rear2)
title('Strain - Rear')
xlabel('Time (sec)')
ylabel(' Strain (micro) ')
xlim ([0.015 0.05])

Front2 = (Front- Front(1)) .*(1000);
t_distance_F = linspace(0,length(Front2)/Fs,length(Front2)); % Creates time vector
figure (14)
plot ( t_distance_F, Front2)
title('Strain - Front ')
xlabel('Time (sec)')
ylabel(' Strain (micro) ')
xlim ([0.015 0.05])

Fs=50000;
Crown2 = (Crown- Crown(1)) .*(1000);
t_distance_C = linspace(0,length(Crown2)/Fs,length(Crown2)); % Creates time vector
figure (15)
plot ( t_distance_C, Crown2)
title('Strain - Crown ')
xlabel('Time (sec)')

```

```
ylabel(' Strain (micro) ' )  
xlim ([0.015 0.05])
```

```
figure (16)  
plot (t_distance_R, Rear2)  
hold on  
plot (t_distance_F, Front2)  
hold on  
plot (t_distance_C, Crown2)  
xlim ([0.015 0.05])  
title('Strain')  
xlabel('Time (sec)')  
ylabel(' Strain (micro) ' )  
legend('Rear','Front','Crown')
```

APPENDIX C

LABVIEW PROGRAM

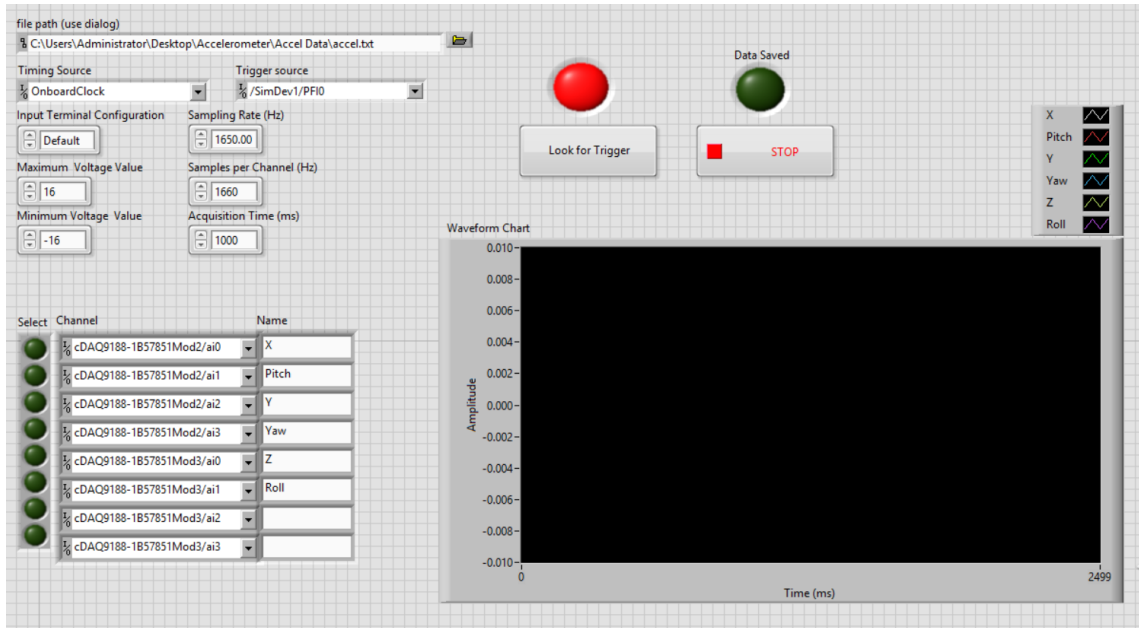


Figure C. 1 LabVIEW Program Front Panel,

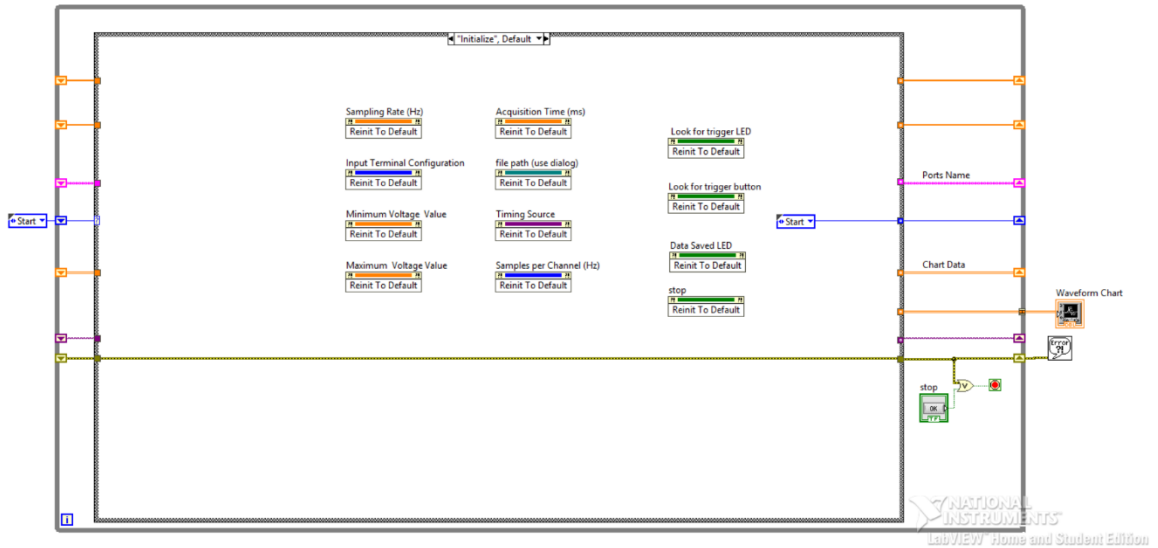


Figure C.2 LabVIEW Block Diagram, first event in the event structure.

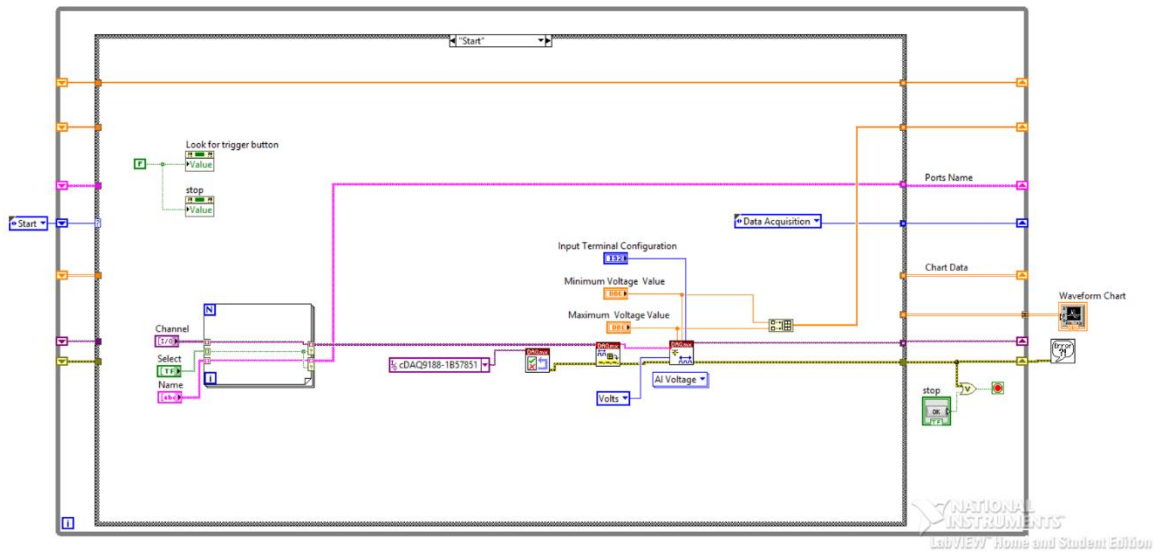


Figure C.3 LabVIEW Block Diagram, second event in the event structure.

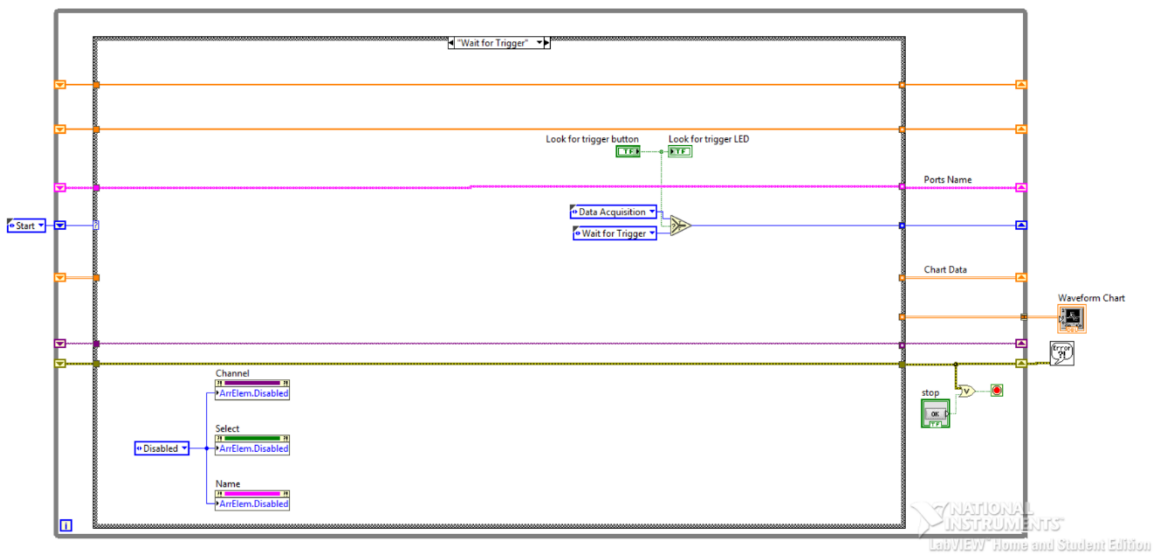


Figure C.4 LabVIEW Block Diagram, third event in the event structure.

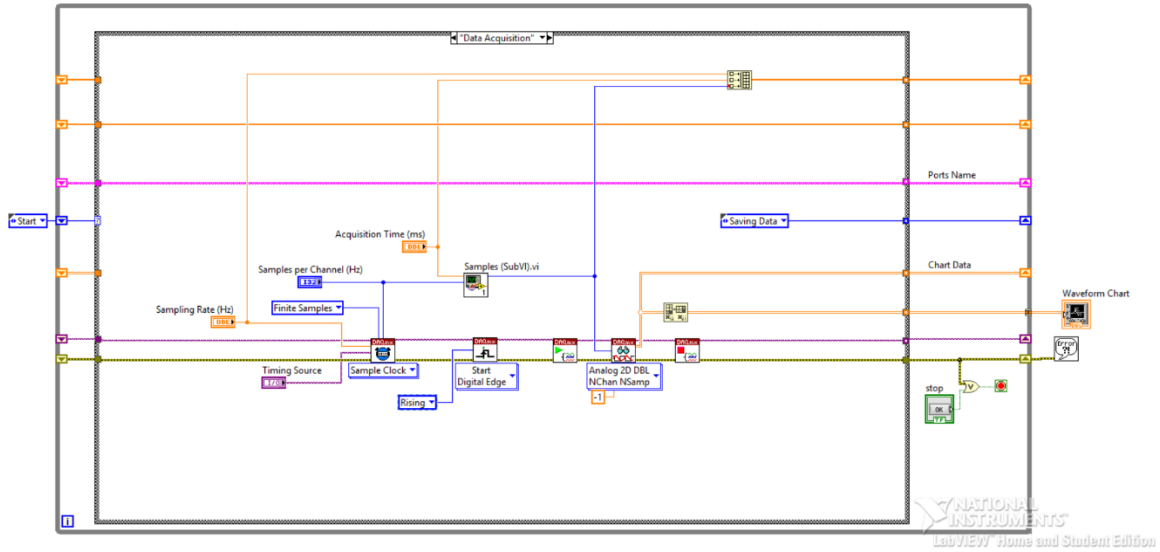


Figure C.5 LabVIEW Block Diagram, fourth event in the event structure.

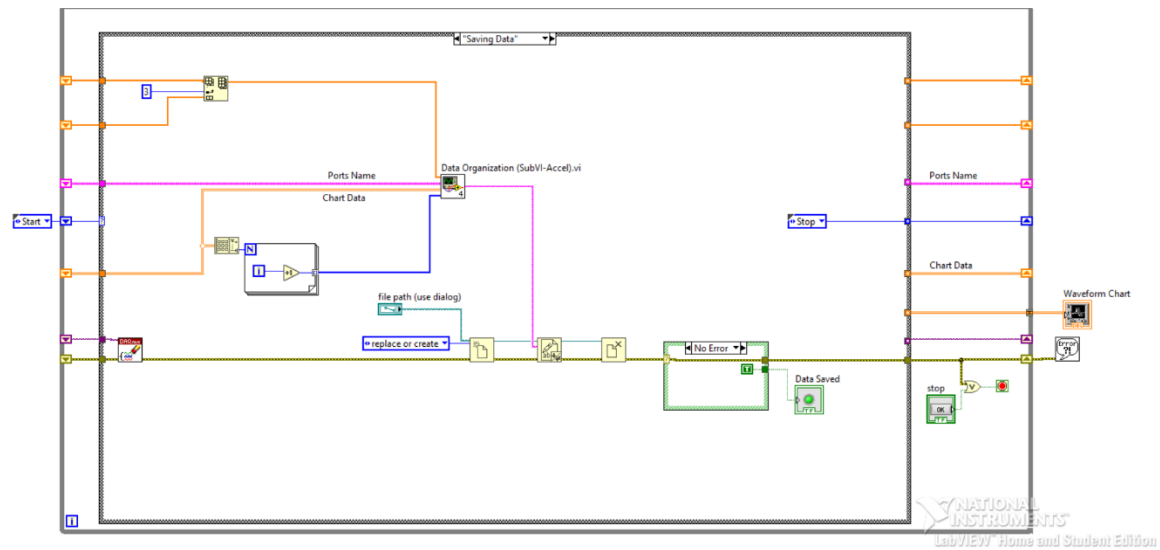


Figure C.6 LabVIEW Block Diagram, fifth event in the event structure.

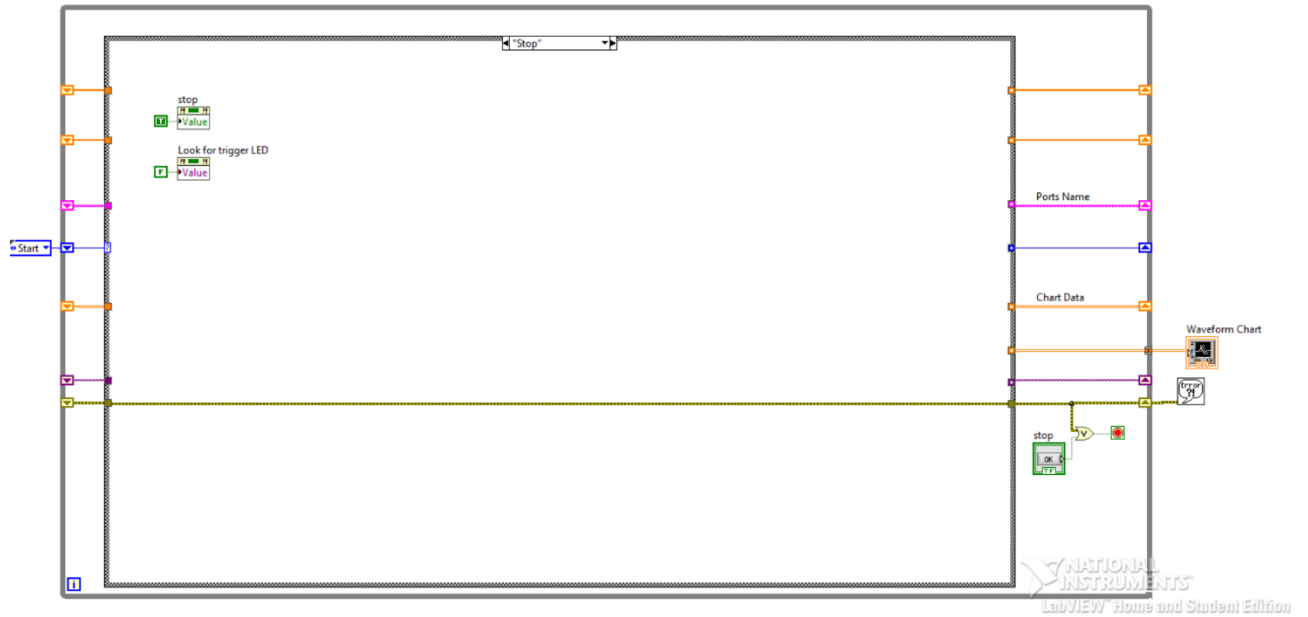


Figure C.7 LabVIEW Block Diagram, sixth event in the event structure.

APPENDIX D

MATLAB SCRIPT 2

The following MATLAB code developed at CIBM3 by Abdus Ali [18] was used to calculate the principle strains developed in the brain surrogate. Modification to code was done to calculate region deformation. Green color suggest note meant for explanation or description of the function being carried out.

```
clear all

clearvars -except dirvideo dirdata*

tracking=
xlsread('D:\07.20\20190506_tes11_all_1.3mps_7.17(20fps)_C001H001S0001\Book1.xls
x','C24:ASA1994'); % Load data
quant_points= size(tracking,2)/2; % # of points in grid
quant_frames=size(tracking,1); % # of frames
clear points_all
for a = 2:2:2*quant_points
    points_all(a/2,,:)= tracking(:,(a-1):a); % xy, # of frames
end

%% Calculations
pointloc_vector_a_all=zeros(quant_points,2);
pointloc_vector_b_all=zeros(quant_points,2);

%% Find nearest coordinates
for point_num=1:quant_points
    pointloc_vector_a_all(point_num,:)= [point_num point_num+1];

    if point_num <=11
        pointloc_vector_b_all(point_num,:)= [point_num point_num+11];

    elseif point_num >=12 && point_num <=23
        pointloc_vector_b_all(point_num,:)= [point_num point_num+12];

    elseif point_num >=24 && point_num <=36
        pointloc_vector_b_all(point_num,:)= [point_num point_num+19];
```

```

elseif point_num >=37 && point_num <=55
    pointloc_vector_b_all(point_num,:)= [point_num point_num+18];

elseif point_num >=56 && point_num <=74
    pointloc_vector_b_all(point_num,:)= [point_num point_num+19];

elseif point_num >=75 && point_num <=93
    pointloc_vector_b_all(point_num,:)= [point_num point_num+19];

elseif point_num >=94 && point_num <=112
    pointloc_vector_b_all(point_num,:)= [point_num point_num+19];

elseif point_num >=113 && point_num <=131
    pointloc_vector_b_all(point_num,:)= [point_num point_num+19];

elseif point_num >=132 && point_num <=150
    pointloc_vector_b_all(point_num,:)= [point_num point_num+17];

elseif point_num >=151 && point_num <=167
    pointloc_vector_b_all(point_num,:)= [point_num point_num+15];

elseif point_num >=168 && point_num <=182
    pointloc_vector_b_all(point_num,:)= [point_num point_num+14];

elseif point_num >=183 && point_num <=195
    pointloc_vector_b_all(point_num,:)= [point_num point_num+11];

elseif point_num >=196 && point_num <=205
    pointloc_vector_b_all(point_num,:)= [point_num point_num+9];

elseif point_num >=206 && point_num <=213
    pointloc_vector_b_all(point_num,:)= [point_num point_num+6];

elseif point_num >=214 && point_num <=216
    pointloc_vector_b_all(point_num,:)= [point_num point_num+4];

elseif point_num >=217 && point_num <=220
    pointloc_vector_b_all(point_num,:)= [point_num point_num-4];

end
end
pointloc_vector_a_all(end,:)= [point_num point_num-1];

for point_num=1:quant_points
    % Create perpendicular vectors a&b

```

```

    vectora= squeeze(points_all(pointloc_vector_a_all(point_num,2),:,:) -
points_all(point_num,:,:));
    vectorb= squeeze(points_all(pointloc_vector_b_all(point_num,2),:,:) -
points_all(point_num,:,:));

    undA= [vectora(:,1) vectorb(:,1)]; % Displacement field at t=0
    clear Eten Eprin
    for frame_num = 1:quant_frames
        F = [vectora(:,frame_num) vectorb(:,frame_num)] / undA; %Deformation gradient
        tensor F= u*inv(u); note B*inv(A) is the same as B/A
        E = ((F' * F) - eye(2))/2; % Eq 3.7 Lagrange strain tensor (C-I)/2
        [eigenvec,eigenval]= eig(E,'vector');

        Eten(:,,frame_num)=E; %strain tensor for all frames
        Eprin(:,,frame_num)=[eigenval; abs(diff(eigenval))]; %principal strains for all
frames

    end
    Eten_all(:,,point_num)=Eten;
    Eprin_all(:,,point_num)=Eprin;

end

%%% Remove these points because they're outside the right,down config for the squares
PointsToRemove= [11 23 36:37 55 74 93 112 131:133 150:152 167:168 182:184
195:196 205:207 212:213 217:220];
Eprin_all(:,,PointsToRemove)=0;
Eten_all(:,,PointsToRemove)=0;

%%% Max principal strains
clear Eprin_max* Eprin_framenum_at_max*
for point_num=1:quant_points
    for strain_num=1:3
        dummy=squeeze(Eprin_all(strain_num,:,point_num));

        %method 1
        if strain_num==1 %compression
            [~,maxframe]=min(dummy);
        else
            [~,maxframe]=max(dummy);
        end
        Eprin_max(point_num,strain_num)=dummy((maxframe));
        Eprin_framenum_at_max(point_num,strain_num)=maxframe;
    end
end

```

```

end
MPSdummy=Eprin_max;

%% Heatmaps MPS,Rate,Impulse
data2plot=MPSdummy;
strain_padded= zeros(300,3);
strain_padded(001:020,:)= vertcat(nan(6,3), squeeze(data2plot(001:011,:)), nan(3,3));
strain_padded(021:040,:)= vertcat(nan(6,3), squeeze(data2plot(012:023,:)), nan(2,3));
strain_padded(041:060,:)= vertcat(nan(6,3), squeeze(data2plot(024:036,:)), nan(1,3));
strain_padded(061:080,:)= vertcat(      squeeze(data2plot(037:055,:)), nan(1,3));
strain_padded(081:100,:)= vertcat(nan(1,3),  squeeze(data2plot(056:074,:)));
strain_padded(101:120,:)= vertcat(nan(1,3),  squeeze(data2plot(075:093,:)));
strain_padded(121:140,:)= vertcat(nan(1,3),  squeeze(data2plot(094:112,:)));
strain_padded(141:160,:)= vertcat(nan(1,3),  squeeze(data2plot(113:131,:)));
strain_padded(161:180,:)= vertcat(nan(1,3),  squeeze(data2plot(132:150,:)));
strain_padded(181:200,:)= vertcat(nan(3,3),  squeeze(data2plot(151:167,:)));
strain_padded(201:220,:)= vertcat(nan(5,3),  squeeze(data2plot(168:182,:)));
strain_padded(221:240,:)= vertcat(nan(6,3),  squeeze(data2plot(183:195,:)), nan(1,3));
strain_padded(241:260,:)= vertcat(nan(8,3),  squeeze(data2plot(196:205,:)), nan(2,3));
strain_padded(261:280,:)= vertcat(nan(9,3),  squeeze(data2plot(206:213,:)), nan(3,3));
strain_padded(281:300,:)= vertcat(nan(11,3), squeeze(data2plot(214:217,:)), nan(5,3));

clear strain_heatmap_min strain_heatmap_mid strain_heatmap_max strain_heatmap
for strain_num=1:3
    strain_heatmap(:,:,strain_num)=vec2mat(strain_padded(:,strain_num),20);
end

figure(2);colormap parula; tally=0;
for strain_num=1:3
    subplot(1,3,strain_num);
    [~, dummyC]= contourf(flipud(strain_heatmap(:,:,strain_num,1)),[-.25:.001:.35]);
    caxis([-0.25 0.35]);set(gca, 'visible', 'off'); set(dummyC, 'LineStyle', 'none');
end

figure(5)
caxis([-0.3 0.31])
colorbar('FontSize',15)

```

REFERENCES

1. Kwong Ming Tse, Siak Piang Lim, Vincent Beng Chye Tan, Heow Pueh Lee (2014, November). *A Review of Head Injury and Finite Element Head Models*. American Journal of Engineering, Technology and Society. Vol. 1, pp. 28-52.
2. Coronado VG, Xu L, Basavaraju SV, McGuire LC, Wald MM, Faul MD, Guzman BR, Hemphill JD (2011, May). *Centers for Disease Control and Prevention (CDC)*. MMWR Surveill Summ. 60(5):1-32.)
3. (2016, January). *Percent Distributions of TBI-related Emergency Department Visits by Age Group and Injury Mechanism — United States, 2006–2010*.
4. Wilberger, J. E., Mao, G. (2017, November) *Traumatic Brain Injury (TBI)*.
5. Post, A., & Hoshizaki, T. B. (2012). *Mechanisms of brain impact injuries and their prediction: a review*. *Trauma*, 14(4), 327-349.
6. Hardy, W. N., Khalil, T. B. and King, A. I. (1994). *Literature review of head injury biomechanics*. *International Journal of Impact Engineering* 15(4), pp. 561-586.
7. Eppinger, R., et al. (1999). *Development of improved injury criteria for the assessment of advanced automotive restraint systems–II*. *National Highway Traffic Safety Administration*, 1-70
8. Martin, P. et al (1998) *Measuring the acceleration of a rigid body* 1-15
9. (2015, July) *Www.micro-measurements.com*, Vishay Precision Instruments, Document number 11092.
10. Prasad Bhatambarekar (2018) *Determining Methods to Reduce Skull Flexure and Brain Deformation*.
11. “Accelerometers.” *Accelerometers: Principle of Operation and Applications*. <https://www.pc-control.co.uk/accelerometers.htm>
12. www.analog.com
13. <https://buy.endevco.com/7264c-accelerometer.html>
14. www.dtsweb.com/angular-rate-ars-pro-hg/
15. David Hazel (2016). *Comparing Strain Gage Measurements to Force Calculations in a Simple Cantilever Beam*.

16. Abdus Ali (2017). *Spatial and Temporal Deformation Pattern of the Brain from Blunt Trauma*, p. 15
17. Murat Eşref Özsüt (2005). *Design and Implementation of LabVIEW Based Data Acquisition and Image Reconstruction Environment for METU-MRI System*, p.26-28.